In-plane structural response and design of duplex and ferritic stainless steel welded I-section beam-columns

Merih Kucukler[a,*], Leroy Gardner[b]

[a]*School of Engineering, University of Warwick, Coventry, CV4 7AL, UK*
[b]*Department of Civil and Environmental Engineering, Imperial College London, London, SW7 2AZ, UK*

Abstract

In this paper, the in-plane behaviour and design of duplex and ferritic stainless steel welded I-section beam-columns fabricated through the welding of individual hot-rolled stainless steel plates are explored. Finite element models able to replicate the structural response of stainless steel I-section members are created and validated against experimental results from the literature. Using the validated finite element models, extensive numerical parametric studies are performed, the results of which are utilised to investigate the accuracy and reliability of existing design provisions for duplex and ferritic stainless steel I-section beam-columns. Scope for improvement is revealed, prompting the development of new beam-column design rules that are compatible with those provided for carbon steel members in EN 1993-1-1. The new proposals are shown to offer improved accuracy and consistency over existing design provisions for duplex and ferritic stainless steel I-section members under combined axial compression and bending, and are recommended for inclusion in the upcoming revision to EN 1993-1-4. The reliability of the proposed design rules, with a partial safety factor $\gamma_{M1} = 1.1$, is demonstrated.

Keywords: Buckling, Beam-columns, Duplex stainless steel, Ferritic stainless steel, I-section, Instability, Numerical modelling, Stainless steel

*Corresponding author
Email addresses: merih.kucukler@warwick.ac.uk (Merih Kucukler), leroy.gardner@imperial.ac.uk (Leroy Gardner)

1. Introduction

The use of stainless steel has been growing in the construction industry owing to its excellent corrosion resistance, high durability, favourable mechanical properties, aesthetic appearance and high strength and stiffness retention in fire. Traditionally, cold-formed stainless steel elements have been the most commonly used stainless steel products in construction, for which extensive research studies have been reported in the literature [1, 2, 3, 4, 5, 6, 7, 8] and comprehensive design guidance is available in structural stainless steel design standards [9, 10, 11, 12]. However, there are increasing demands for higher load carrying capacities for stainless steel structural elements, which can be fulfilled through the use of I-section members fabricated through the welding of individual plates. However, thus far, the structural response and design of welded stainless steel I-section members have been far less extensively explored relative to cold-formed stainless steel members, signifying the need for research in this area.

The behaviour of stainless steel I-section members has been examined in a number of previous studies. Burgan et al. [13], Zheng et al. [14], Ahmed et al. [15] and Yang et al. [16, 17] carried out a series of physical experiments on arc-welded austenitic and duplex stainless steel I-section columns and beam-columns. Yuan et al. [18] put forward residual stress patterns for arc-welded austenitic, duplex and ferritic stainless steel I-sections. Bredenkamp and Van der Berg [19] tested a series of arc-welded ferritic stainless steel I-section columns. In Yang et al. [20] and Wang et al. [21], physical experiments were performed on arc-welded austenitic stainless steel I-section beams susceptible to lateral-torsional buckling. Saliba and Gardner [22] and Yuan et al. [23] explored the cross-section response of arc-welded stainless steel I-sections. Gardner et al. [24] initiated a research programme into the behaviour and design of austenitic stainless steel I-section members fabricated through laser-welding, which has resulted in the development of residual stress patterns [24], column design rules [25], design rules for the determination of cross-section bending moment resis-

tances [26] and a beam-column design method [27] for laser-welded austenitic stainless steel I-section elements. Building upon these studies [24, 25, 26, 27], Kucukler et al. [28] explored the structural response of laser-welded austenitic stainless steel I-section beam-columns susceptible to flexural-torsional buckling and developed design guidance for such members, which are due to appear in the upcoming version of the European structural stainless steel design standard EN 1993-1-4 [9]. While there has been a recent increase in research studies into the structural response of stainless steel I-section members, the previous studies have predominantly focused on austenitic stainless steel I-section elements; the behaviour and design of duplex and ferritic stainless steel I-section members are therefore the focus of the present study.

A programme of research into the structural response of duplex and ferritic stainless steel I-section members has been initiated by Kucukler [29], focusing in the first instance on columns and establishing new flexural buckling curves that provide more accurate ultimate strength predictions than given by existing column design rules [9, 10, 11, 12]. Building upon this initial research, the present study explores the structural response of duplex and ferritic stainless steel I-section members subjected to combined major or minor axis bending and axial compression. Finite element models able to simulate the behaviour of duplex and ferritic stainless steel I-section beam-columns are developed and validated against experimental results from the literature. Using the developed finite element (FE) models, which are analysed considering both geometrical and material nonlinearities with imperfections (GMNIA), extensive numerical parametric studies are conducted, covering a broad range of cross-section proportions, member slendernesses and loading conditions. The FE results, as well as existing tests results, are used to assess the accuracy of the current design rules for duplex and ferritic stainless steel I-section beam-columns given in the European structural stainless steel design standard EN 1993-1-4 [9] and the North American stainless steel design guide AISC Design Guide 27 [10]. The proposals of Greiner and Kettler [30] are

also assessed. Shortcomings in the existing design provisions are revealed, prompting the development of a new design approach, compatible with the beam-column design rules given EN 1993-1-1 [31], and resulting in improved accuracy for the design of duplex and ferritic stainless steel I-section beam-columns. The reliability of the proposed design approach is also illustrated.

2. Numerical modelling

2.1. Introduction

In this section, finite element modes able to mimic the structural response of stainless steel I-section members are developed and validated against experimental results from the literature. Numerical parametric studies, performed through the GMNIA of the validated finite element models, are then presented.

2.2. Element type and modelling assumptions

The finite element models were created using the finite element analysis software Abaqus [32]. The four-noded reduced integration general purpose shell finite element referred to as S4R, which has been successfully used in similar applications [33, 34, 35, 36, 37], was utilised to establish all the finite element models in this paper. 16 elements were used to mesh each flange and web plate of the modelled I-sections in order to capture local buckling and the spread of plasticity through the cross-section depth accurately. The web plates were offset by half the flange thicknesses so that overlapping of the flange and web plates was avoided. The number of the finite elements along the member lengths was selected such that the aspect ratios of the elements within the web were approximately equal to unity. The default Simpson integration method with five integration points through the thickness of each finite element was adopted. The Poisson's ratio was taken as 0.3 in the elastic range and 0.5 in the plastic range by defining the effective Poisson's ratio as 0.5 to allow for the change

of cross-sectional area under load. The von Mises yield criterion with the associated flow rule and isotropic hardening were adopted in the finite element models. The engineering stress-strain ($\sigma - \epsilon$) response of stainless steel was defined using the two stage compound Ramberg-Osgood material model [38, 39], illustrated in Fig. 1 (a), as given by eqs. (1) and (2):

$$\epsilon = \frac{\sigma}{E} + 0.002 \left(\frac{\sigma}{f_y}\right)^n \quad \text{for} \quad \sigma \leq f_y, \tag{1}$$

$$\epsilon = \frac{\sigma - f_y}{E_{p0.2}} + \left(\epsilon_u - \epsilon_{p0.2} - \frac{f_u - f_y}{E_{p0.2}}\right) \left(\frac{\sigma - f_y}{f_u - f_y}\right)^m + \epsilon_{p0.2} \quad \text{for} \quad f_y < \sigma \leq f_u, \tag{2}$$

where n and m are strain hardening exponents, f_y is the yield stress taken as the 0.2% proof stress, E is the Young's modulus, $E_{p0.2}$ and $\epsilon_{p0.2}$ are the tangent modulus and total strain at the 0.2% proof stress f_y respectively, and f_u and ϵ_u are the ultimate tensile strength and strain. In this study, the standardised material properties for hot-rolled duplex and ferritic stainless steel plates given by [40] were utilised to define the material properties of the modelled I-section members. The resulting values of f_y, f_u, ϵ_u, n and m are provided in Table 1, while the engineering stress-strain curves are shown in Fig. 1 (b). Since the constitutive formulations of Abaqus [32] adopt the Cauchy (true) stress-strain assumption for the adopted shell element type, the engineering stress-strain response shown in Fig. 1 (b) was transformed into the true stress-log plastic strain response (σ_{true}-ϵ^{pl}_{true}) and input into Abaqus [32].

Pin-ended support conditions were established in the finite element models through kinematic coupling constraints, constraining the degrees of freedoms of the nodes within the end section to a reference point located at the centroid of the cross-section where pin-ended boundary conditions were defined. Axial compression N_{Ed} and bending moments M_{Ed} were applied simultaneously within the same step at the reference points during the analyses of the finite element models; a range of axial force to bending moment ratios was considered.

The beam-columns subjected to major axis bending plus axial compression were laterally restrained along their lengths at the web-to-flange junctions to suppress the influence of flexural-torsional buckling, which is outside the scope of the present study and will be considered in future work.

2.3. Geometric imperfections

Global and local geometric imperfections were applied to the finite element models in the form of buckling modes determined through Linear Buckling Analysis (LBA), as shown in Fig. 2 and Fig. 3 for beam-columns under major axis bending plus compression and minor axis bending plus compression, respectively. In the application of the local geometric imperfections, the lowest local buckling modes were scaled to 80% of the fabrication tolerances for welded steel members provided in EN 1090-2 [41], in line with the recommendations of EN 1993-1-5 [42]. Thus, the lowest local buckling modes were scaled to 80% of 1/100 of the web height h_w (i.e. $\omega_l = 0.8h_w/100$) when the maximum normalised displacement from the LBA arose within the web, while the lowest local buckling modes were scaled to 80% of 1/100 of the flange width b when the maximum normalised buckling displacement from the LBA arose within the flanges (i.e. $\omega_l = 0.8b/100$). These imperfection amplitudes represent an approximate upper bound to the amplitudes likely to be observed in practice and were found to be safe-sided relative to the measurements on stainless steel welded I-sections in Gardner et al. [24]. For the global geometric imperfections, the amplitudes ω_g were taken as 1/1000 of the length L of the stainless steel beam-columns (i.e. $\omega_g = L/1000$) in accordance with the recommendations of [41].

2.4. Residual stresses

Membrane residual stresses were applied to the finite element models using the pattern put forward by Yuan et al. [18] for arc-welded duplex and ferritic stainless steel I-sections, which is illustrated in Fig. 4; note that the weld geometry was not explicitly modelled in

line with previous studies [43, 44] owing to its relatively small influence, dependency on the welding process and, for consistency, exclusion from the geometric properties employed in the analysis of the results and assessment of the resistance functions in Sections 3-5. As can be seen in Fig. 4, the maximum tensile residual stresses within the flanges σ_{ft} and web σ_{wt} are equal to 60% of the 0.2% proof stress f_y (i.e. $\sigma_{ft} = \sigma_{wt} = 0.6f_y$). The maximum compressive residual stresses in the flanges σ_{fc} and web σ_{wc} are determined considering axial force equilibrium within the cross-section. The residual stress pattern shown in Fig. 4 was applied to the finite element models in a step-wise fashion by defining constant values (taken at the middle of each element) of residual stress at the element integration points. Since membrane residual stresses are dominant in welded sections [18], through thickness stress variations (i.e. bending residual stresses) were not considered. The residual stresses were applied to the finite element models within a separate analysis step, which was performed prior to the application of the external loading. Since stainless steel has a nonlinear material stress-strain response, the application of the residual stresses results in the development of permanent strains; corresponding residual plastic strains $\epsilon_{res,pl}$ were thus also applied to the finite element models. In accordance with the two stage Ramberg-Osgood material model defined by eq. (1) and eq. (2), the residual plastic strains $\epsilon_{res,pl}$ were defined at the cross-section integration points of the finite element models using the following expression [45]:

$$\epsilon_{res,pl} = 0.002 \left(\frac{\sigma_{res}}{f_y} \right)^n, \tag{3}$$

where σ_{res} is the residual stress applied at the considered cross-section integration point and n is the Ramberg-Osgood exponent, the values of which are provided in Table 1 for duplex and ferritic stainless steel. It should be noted that the application of the residual plastic strains $\epsilon_{res,pl}$ to the finite element models is required to enable the achievement of the desired

residual stress pattern shown in Fig. 4 after the equilibrium load step.

2.5. Validation of numerical models

The finite element models developed herein were validated against the experimental results reported in [17], where twenty full-scale physical tests were performed on stainless steel welded I-section beam-columns. In the experiments, ten grade 1.4462 duplex stainless steel and ten grade 1.4301 austenitic stainless steel I-section beam-column specimens were tested. In both cases, half of the specimens were subjected to major axis bending plus axial compression and the other half were subjected to minor axis bending and axial compression. The combination of bending and axial compression was achieved by applying the load at eccentricities of between 40 mm and 70 mm. Pin-ended support conditions were achieved by means of knife edges at the specimen ends, thereby enabling free rotations about the axis of bending at the end sections; hence, the effective buckling lengths of the specimens L_{cr} were taken equal to their actual lengths L plus the thickness of the two knife edges (170 mm each), i.e. $L_{cr} = L + 340$ mm. For the validation of the finite element models, the material and geometric properties of the specimens reported in [17] and the residual stress pattern recommended in [18] were adopted. Since the local geometric imperfections of the specimens were not measured in [17], the magnitudes of the local geometric imperfections were taken as 80% of the fabrication tolerances for welded steel sections given in [41]. For the global geometric imperfections, both the maximum values measured in [17] $\omega_g = e_{0,m}$ and the values of $\omega_g = L/1000$ were applied in turn to the finite element models. The imperfection shapes were taken as the lowest local and global buckling modes of the specimens. Coupling constraints were utilised in the definition of the end support conditions of the finite element models; the degrees of the freedom of all the nodes within the end sections were coupled to eccentric reference points where loading was applied and pin-ended boundary conditions were defined. The eccentric reference points were offset longitudinally by 170 mm from the specimen ends to represent the thickness of the knife edges and transversely from

the centroids of the end-sections considering the corresponding eccentricity values adopted during the experiments, thereby enabling the application of combined bending and axial compression to the finite element models.

Tables 2 and 3 show comparisons of the ultimate resistances of the specimens observed during the experiments of Yang et al. [17] $N_{ult,exp}$ and those obtained through the finite element models created in this study $N_{ult,FE}$. In the tables, the specimens with 2205 in their designation are made of grade 1.4462 duplex stainless steel and those with 304 in their designation are made of grade 1.4301 austenitic stainless steel. Furthermore, $\overline{\lambda}_y = \sqrt{Af_y/N_{cr,y}}$ and $\overline{\lambda}_z = \sqrt{Af_y/N_{cr,z}}$ are the non-dimensional major and minor axis flexural buckling slendernesses, where A is the cross-section area, f_y is the 0.2% proof strength and $N_{cr,y}$ and $N_{cr,z}$ are the elastic critical buckling loads corresponding to the major and minor axes, respectively. As can be seen from Tables 2 and 3, the finite element models provide ultimate resistances that are close to, but on the safe side of, those obtained during the experiments, indicating that the models are able to replicate the structural response of the stainless steel welded I-section beam-columns accurately. The discrepancies between the ultimate strengths obtained from the experiments and those predicted by the finite element models are ascribed to the differences in the shapes and magnitudes of the local and global geometric imperfections of the specimens and those adopted in this study. Table 2 and Table 3 also show that the differences between the ultimate capacities obtained adopting the maximum global geometric imperfection magnitudes measured for the test specimens $\omega_g = e_{0,m}$ and those determined using the fabrication tolerance values of $\omega_g = L/1000$ are generally small. Comparisons of the load versus mid-height lateral deformation paths of the specimens observed during the experiments and those determined through the finite element models are shown in Fig. 5 and Fig. 6, where it can be seen that there is generally good correlation between the two, though the FE models exhibit somewhat sharper post-peak unloading in Fig. 5. This is attributed to the development of more severe and concentrated local buck-

ling caused by the adopted eigenmode affine local imperfection shapes. The failure modes of specimens I 304-2500 and H 304-2500 observed during the experiments and those determined through the finite element models are compared in Figs. 7 and 8, again showing good agreement between the two. Overall, it can be concluded that the developed finite element models are capable of accurately predicting the observed physical response of stainless steel welded I-section beam-columns. The same finite element modelling approach has also been extensively validated in previous investigations [28, 29] and is thus considered to be suitable for performing parametric studies.

2.6. Parametric studies

Following the validation of the adopted finite element modelling approach, extensive numerical parametric studies were carried out, as reported in this section. A summary of the numerical parametric studies performed for duplex and ferritic stainless welded I-section beam-columns is illustrated in Table 4. As can be seen from the table, the finite element models were subjected to both combined axial compression N_{Ed} and major axis bending $M_{y,Ed}$ and combined axial compression N_{Ed} and minor axis bending moments $M_{z,Ed}$. Five different ratios of normalised applied bending moment $M_{Ed}/(W_{pl}f_y)$ to applied axial force $N_{Ed}/(Af_y)$ were considered, where W_{pl} is the the plastic section modulus, A is the cross-section area and f_y is the 0.2% proof strength. In accordance with Kucukler et al. [28], a constant cross-section depth h equal to 50 mm (i.e. $h = 50$ mm) was used in the parametric studies, while the cross-sections widths b were varied such that the aspect ratios h/b of the sections were equal to 1.0, 1.5, 2.0 and 3.0 (i.e. $h/b = 1.0, 1.5, 2.0$ and 3.0). For each cross-section aspect ratio, three different values of flange thickness t_f and web thickness t_w were selected, thereby creating cross-sections with a range of cross-section slendernesses falling into the Class 1, Class 2 and Class 3 categories according to EN 1993-1-4 [9]. The thicknesses of the web and flange plates of the cross-sections were specified such that the web plate slenderness $\overline{\lambda}_{p,w}$ and the flange plate slenderness $\overline{\lambda}_{p,f}$ were essentially equal; the

web and flange plate slendernesses were determined from eq. (4) and eq. (5):

$$\overline{\lambda}_{p,w} = \sqrt{f_y / f_{cr,w}}, \tag{4}$$

$$\overline{\lambda}_{p,f} = \sqrt{f_y / f_{cr,f}}, \tag{5}$$

in which $f_{cr,w}$ and $f_{cr,f}$ are the elastic local buckling stresses of the web and flange plates considered in isolation, respectively. Beam-columns with seven different lengths L were modelled for each cross-section; the lengths of the beam-columns were selected such that the non-dimensional flexural buckling slenderness $\overline{\lambda}$ of the beam-columns ranged between 0.4 and 2.0 in increments of 0.4. Two additional lengths corresponding to $\overline{\lambda} = 0.2$ and $\overline{\lambda} = 1.0$ were also taken into consideration for each cross-section. Note that $\overline{\lambda}$ is taken as the flexural buckling slenderness about the major axis for the beam-columns under major axis bending and axial compression (i.e. $\overline{\lambda} = \overline{\lambda}_y$), while it is taken as the flexural buckling slenderness about the minor axis for the beam-columns subjected to minor axis bending plus axial compression (i.e. $\overline{\lambda} = \overline{\lambda}_z$). In total, the GMNIA of 840 stainless steel I-section beam-columns were performed in the numerical parametric studies. In the following sections, the structural performance data generated through the extensive numerical parametric studies are used (i) to assess the accuracy of the existing design methods for duplex and ferritic stainless steel I-section beam-columns and (ii) to establish a new beam-column design method leading to more accurate resistance predictions.

3. Assessment of existing design rules for duplex and ferritic stainless steel I-section beam-columns

3.1. Introduction

In this section, the accuracy of the existing design methods for duplex and ferritic stainless steel welded I-section beam-columns provided in (i) the European structural stainless

steel design standard EN 1993-1-4 [9], (ii) AISC Design Guide 27 [10] and (iii) the study of Greiner and Kettler [30] is investigated using the numerical results obtained in the present investigation and the experimental results obtained from [17]. As shown in Fig. 9, the parameter ϵ is defined as the ratio of the ultimate load determined from each numerical model or experiment N_u to that obtained from the design method $N_{u,pred}$; this ratio is used to assess the accuracy of each design method (i.e. $\epsilon = N_u/N_{u,pred}$), where it is assumed that the beam-columns are under proportional loading. In Fig. 9, $N_{b,Rd}$ and M_{Rd} are the column buckling and bending moment resistances calculated using each design method and represent the end points of the design interaction curve, N_{Ed} and M_{Ed} are the proportionally increasing axial compression and bending moment, and θ is the radial angle specifying the relationship between the applied axial compression and bending moment and determined through the following equation:

$$\theta = tan^{-1}\left(\frac{N_{Ed}/N_{b,Rd}}{M_{Ed}/M_{Rd}}\right). \tag{6}$$

As can been in Fig. 9, the radial angle varies between 0° and 90° depending on the dominance of the applied axial compression and bending; $\theta = 0°$ and $\theta = 90°$ correspond to pure bending and axial compression, respectively. A safe-sided ultimate strength prediction is signified by values of $\epsilon = N_u/N_{u,pred}$ greater than 1.0.

The assessment of the accuracy of EN 1993-1-4 [9], AISC Design Guide 27 [10] and the proposals of Greiner and Kettler [30] is provided in Table 5 and in Table 6 for duplex and ferritic stainless steel sections beam-columns, respectively. In the assessment of the accuracy of the existing design methods, the numerical results obtained through the parametric studies carried out in this paper for duplex and ferritic stainless steel beam-columns and the experimental results obtained in the experiments of [17] for duplex stainless steel beam-columns were utilised. In Tables 5 and 6, ϵ_{av}, ϵ_{COV}, ϵ_{max} and ϵ_{min} correspond to the average,

coefficient of variation, maximum and minimum of ϵ values obtained for a design method. The partial safety factors γ_M and resistance factors ϕ were taken equal to 1.0 in the determination of the ultimate strengths of stainless steel beam-columns using EN 1993-1-4 [9] and AISC Design Guide 27 [10], respectively. In the following sections, the three beam-column design methods considered in this study are briefly described and the accuracy of the design methods for duplex and ferritic stainless steel I-section beam-columns is investigated.

3.2. European structural stainless steel design code EN 1993-1-4 [9]

In the European structural stainless steel design standard EN 1993-1-4 [9], the following equation is provided for the design of laterally restrained stainless steel I-section beam-columns not susceptible to flexural-torsional buckling and under uniaxial major axis bending moment and axial compression:

$$\frac{N_{Ed}}{(N_{b,Rd})_{min}} + k_y \left(\frac{M_{y,Ed} + N_{Ed} e_{Ny}}{\beta_{w,y} W_{pl,y} f_y / \gamma_{M1}} \right) \leq 1.0, \tag{7}$$

and the following equation is given for the design of beam-columns under uniaxial minor axis bending moment plus axial compression:

$$\frac{N_{Ed}}{(N_{b,Rd})_{min}} + k_z \left(\frac{M_{z,Ed} + N_{Ed} e_{Nz}}{\beta_{w,z} W_{pl,z} f_y / \gamma_{M1}} \right) \leq 1.0. \tag{8}$$

In eq. (7) and eq. (8), N_{Ed}, $M_{y,Ed}$ and $M_{z,Ed}$ are the design values of axial compression, major axis bending moment and minor axis bending moment respectively, $(N_{b,Rd})_{min}$ is the smallest design column buckling resistance determined considering flexural buckling about the major axis and minor axis, torsional buckling and torsional flexural buckling, e_{Ny} and e_{Nz} are the shifts in the neutral axis when the cross-section is subjected to uniform axial compression, which are equal to zero for I-sections, and $W_{pl,y}$ and $W_{pl,z}$ are the plastic section moduli about the major axis and minor axis. Additionally, $\beta_{w,y}$ and $\beta_{w,z}$ are auxiliary coefficients,

which are equal to 1.0 for Class 1 and 2 cross-sections, the ratios between the elastic section $W_{el,y}$, $W_{el,z}$ and plastic section moduli $W_{pl,y}$, $W_{pl,z}$ about the major and minor axes for Class 3 cross-sections (i.e. $\beta_{w,y} = W_{el,y}/W_{pl,y}$ and $\beta_{w,z} = W_{el,z}/W_{pl,z}$), and the ratios between the effective section $W_{el,y}$, $W_{el,z}$ and plastic section moduli $W_{pl,y}$, $W_{pl,z}$ about the major and minor axes for Class 4 cross-sections (i.e. $\beta_{w,y} = W_{eff,y}/W_{pl,y}$ and $\beta_{w,z} = W_{eff,z}/W_{pl,z}$). Finally, k_y and k_z in eqs. (7) and (8), respectively, are the interaction factors, calculated as:

$$k_y = 1 + 2\left(\overline{\lambda}_y - 0.5\right)\frac{N_{Ed}}{N_{b,Rd,y}} \qquad \text{but} \qquad 1.2 \leq k_y \leq 1.2 + 2\frac{N_{Ed}}{N_{b,Rd,y}}, \tag{9}$$

$$k_z = 1 + 2\left(\overline{\lambda}_z - 0.5\right)\frac{N_{Ed}}{\left(N_{b,Rd}\right)_{min,1}} \qquad \text{but} \qquad 1.2 \leq k_y \leq 1.2 + 2\frac{N_{Ed}}{\left(N_{b,Rd}\right)_{min,1}} \tag{10}$$

where $N_{b,Rd,y}$ is the column major axis flexural buckling resistance and $\left(N_{b,Rd}\right)_{min,1}$ is the column resistance determined considering flexural buckling about the minor axis, torsional buckling and torsional-flexural buckling.

In Fig. 10, the accuracy of the current beam-column design rules of EN 1993-1-4 [9] is illustrated for duplex and ferritic stainless steel I-section members under major axis bending and axial compression and minor axis bending and axial compression, where the ratios of the numerically and experimentally obtained ultimate strengths N_u to those determined through the beam-column design rules of EN 1993-1-4 [9] $N_{u,EC3}$ (i.e. $N_u/N_{u,EC3}$) are plotted against the radial angles θ calculated considering the design interaction curves of EN 1993-1-4 [9] as shown in Fig. 9. Note that in Fig. 10, the design column buckling resistances are determined through the existing column design rules of [9]. The accuracy of EN 1993-1-4 [9] is also assessed in Tables 5 and 6. The results provided in Fig. 10, Table 5 and Table 6 indicate that the EN 1993-1-4 [9] beam-column design provisions generally yield rather scattered and overly-conservative ultimate strength predictions for duplex and ferritic stainless steel I-section beam-columns.

3.3. AISC Design Guide 27 [10]

The North American structural stainless steel design guide AISC Design Guide 27 [10] recommends the use of the following design equations for stainless steel I-section beam-columns

$$\frac{N_{Ed}}{N_b} + \frac{8}{9}\left(\frac{M^{II}_{y,Ed}}{M_{y,b}} + \frac{M^{II}_{z,Ed}}{M_{z,c}}\right) \leq 1.0 \qquad \text{if} \qquad \frac{N_{Ed}}{N_b} \geq 0.2, \tag{11}$$

$$\frac{N_{Ed}}{2N_b} + \left(\frac{M^{II}_{y,Ed}}{M_{y,b}} + \frac{M^{II}_{z,Ed}}{M_{z,c}}\right) \leq 1.0 \qquad \text{if} \qquad \frac{N_{Ed}}{N_b} < 0.2 \tag{12}$$

in which N_b and $M_{y,b}$ are the column and beam buckling resistances, $M_{z,c}$ is the minor axis cross-section bending moment resistance and $M^{II}_{y,Ed}$ and $M^{II}_{z,Ed}$ are the maximum values of the bending moments about the y and z axes along the member lengths, determined considering second-order $P-\delta$ and $P-\Delta$ effects. Note that for a beam-column that is not susceptible to flexural-torsional buckling, $M_{y,b}$ is equal to the major axis cross-section bending moment resistance $M_{y,c}$ (i.e. $M_{y,b} = M_{y,c}$).

The accuracy of AISC Design Guide 27 [10] for the design of duplex and ferritic stainless steel beam-columns is provided in Fig. 11 and in Tables 5 and 6. As can be seen from the figure, AISC Design Guide 27 [10] provides rather scattered ultimate strength predictions for duplex and ferritic stainless steel I-section columns and its accuracy is lower than that of EN 1993-1-4 [9].

3.4. Greiner and Kettler [30] proposal

In Greiner and Kettler [30], a design method for stainless steel I-section beam-columns with Class 1 and 2 cross-sections was put forward, using the format adopted for the beam-column design equations of the European structural carbon steel design standard EN 1993-1-1 [31]. The following beam-column design equations are recommended in [30] for laterally restrained stainless steel I-section beam-columns subjected to axial compression plus major

axis bending:

$$\frac{N_{Ed}}{N_{b,y,Rd}} + k_{y,G\&K}\frac{M_{y,Ed}}{W_{pl,yf_y}} \leq 1.0, \tag{13}$$

and for stainless steel beam-columns under minor axis bending plus axial compression:

$$\frac{N_{Ed}}{N_{b,z,Rd}} + k_{z,G\&K}\frac{M_{y,Ed}}{W_{pl,zf_y}} \leq 1.0. \tag{14}$$

In eq. (13) and eq. (14), $N_{b,z,Rd}$ is the column minor axis buckling resistance determined considering flexural buckling about the minor axis buckling, torsional buckling and torsional-flexural buckling and $k_{y,G\&K}$ and $k_{z,G\&K}$ are the interaction factors calculated as given below:

$$k_{y,G\&K} = 0.9 + 2.2\frac{N_{Ed}}{N_{b,y,Rd}}\left(\overline{\lambda}_y - 0.4\right) \quad \text{but} \quad k_{y,G\&K} \leq 0.9 + 2.942\frac{N_{Ed}}{N_{b,y,Rd}}, \tag{15}$$

$$k_{z,G\&K} = 1.2 + 1.5\frac{N_{Ed}}{N_{b,z,Rd}}\left(\overline{\lambda}_z - 0.7\right) \quad \text{but} \quad k_{z,G\&K} \leq 1.2 + 1.95\frac{N_{Ed}}{N_{b,z,Rd}}. \tag{16}$$

Fig. 12 shows the accuracy of the beam-column design method put forward by Greiner and Kettler [30] for duplex and ferritic stainless steel I-section beam-columns. A numerical assessment is also presented in Tables 5 and 6. As can be seen from Fig. 12 and Tables 5 and 6, relative to EN 1993-1-4 [9] and AISC Design Guide 27 [10], the beam-column design method of Greiner and Kettler [30] leads to more accurate ultimate strength predictions for duplex and ferritic stainless steel welded I-section beam-columns, though there still remains scope for improvement; this design method is also not applicable to beam-columns with Class 3 cross-sections.

4. New proposal for in-plane design of stainless steel welded I-section beam-columns

4.1. Introduction

The assessment of the existing design methods for duplex and ferritic stainless steel I-section beam-columns in the previous section indicated that the existing design methods lead to somewhat inaccurate and scattered ultimate strength predictions. New design rules for duplex and ferritic stainless steel welded I-section beam-columns are presented and assessed in this section. In line with [28, 27], the general format of the beam-column interaction equations of EN 1993-1-1 [31] have been adopted herein in the development of the proposed design method, seeking improved resistance predictions through (i) the adoption of more accurate end-points of the interaction curves (i.e. the column buckling and cross-section bending moment resistances) and (ii) the establishment of new interaction factors providing beam-column design interaction curves that predict more accurately the ultimate strengths of duplex and ferritic stainless steel I-section beam-columns.

4.2. New interaction equations

The following interaction equations are proposed for the design of duplex and ferritic stainless steel welded I-section beam-columns subjected to major axis bending plus axial compression and restrained against lateral-torsional buckling:

$$\frac{N_{Ed}}{N_{b,y,Rd}} + k_{y,prop}\frac{M_{y,Ed}}{M_{y,csm,Rk}/\gamma_{M1}} \leq 1.0, \tag{17}$$

and for those under combined minor axis bending and axial compression:

$$\frac{N_{Ed}}{N_{b,z,Rd}} + k_{z,prop}\frac{M_{z,Ed}}{M_{z,csm,Rk}/\gamma_{M1}} \leq 1.0, \tag{18}$$

in which $k_{y,prop}$ and $k_{z,prop}$ are the interaction factors calibrated in this section, γ_{M1} is the partial safety factor for member buckling resistance and $M_{y,csm,Rk}$ and $M_{z,csm,Rk}$ are the major and minor axis cross-section bending moment resistances determined according to the continuous strength method (CSM), respectively. The following formulae are used for the determination of the major axis cross-section bending moment resistance $M_{y,csm,Rk}$:

$$M_{y,csm,Rk} = W_{pl,y} f_y \left[1 + \frac{E_{sh}}{E} \frac{W_{el,y}}{W_{pl,y}} \left(\frac{\epsilon_{csm}}{\epsilon_y} - 1 \right) - \left(1 - \frac{W_{el,y}}{W_{pl,y}} \right) / \left(\frac{\epsilon_{csm}}{\epsilon_y} \right)^2 \right], \tag{19}$$

and for the determination of the minor axis cross-section bending moment resistance $M_{z,csm,Rk}$:

$$M_{z,csm,Rk} = W_{pl,z} f_y \left[1 + \frac{E_{sh}}{E} \frac{W_{el,z}}{W_{pl,z}} \left(\frac{\epsilon_{csm}}{\epsilon_y} - 1 \right) - \left(1 - \frac{W_{el,z}}{W_{pl,z}} \right) / \left(\frac{\epsilon_{csm}}{\epsilon_y} \right)^{1.2} \right] \tag{20}$$

according to the CSM, where W_{pl} and W_{el} are the plastic and elastic section moduli, $E_{sh} = (f_u - f_y)/(C_2\epsilon_u - \epsilon_y)$ is the slope of the strain hardening range in the CSM material model with $C_2 = 0.16$ for duplex stainless steel and $C_2 = 0.45$ for ferritic stainless steel, ϵ_{csm} is the failure strain of the cross-section determined through the CSM base curve [46] and ϵ_y is the yield strain. The derivation of eq. (19) and eq. (20) and further information about the CSM are provided in [47, 46, 48].

For the determination of the column buckling resistances, in line with EN 1993-1-4 [9] and Kucukler [29], the use of the Perry-Robertson column buckling equation is recommended, as given by:

$$N_{b,Rd} = \frac{\chi A f_y}{\gamma_{M1}}, \tag{21}$$

where χ is the column buckling reduction factor determined as:

$$\chi = \frac{1}{\phi + \sqrt{\phi^2 - \overline{\lambda}^2}} \quad \text{where} \quad \phi = 0.5\left[1 + \alpha\left(\overline{\lambda} - \overline{\lambda}_0\right) + \overline{\lambda}^2\right] \tag{22}$$

in which α and $\overline{\lambda}_0$ are the imperfection factor and threshold slenderness below which $\chi = 1.0$, respectively. In Kucukler et al. [29], new column buckling curves leading to more accurate ultimate strength predictions for duplex and ferritic stainless steel I-section columns relative to those obtained through the existing column buckling curves of EN 1993-1-4 [9] were derived. The new calibrated values of α and $\overline{\lambda}_0$ derived in Kucukler [29] are provided in Table 7 for the major and minor axis buckling assessment of duplex and ferritic stainless steel I-section beam-columns. Note that the major $N_{b,y,Rd}$ and minor axis $N_{b,z,Rd}$ column buckling resistances used in eq. (17) and eq. (18) are determined through eq. (21), using the corresponding values of α and $\overline{\lambda}_0$ given in Table 7 and the corresponding major axis $\overline{\lambda}_y$ and minor axis $\overline{\lambda}_z$ non-dimensional slendernesses.

4.3. Calibration of interaction factors

Utilising the CSM cross-section bending moment resistances $M_{y,csm,Rk}$ and $M_{z,csm,Rk}$ and the new column buckling curves derived in [28], which lead to more accurate predictions of the end-points of the interaction curves, new interaction factors $k_{y,prop}$ and $k_{z,prop}$ are calibrated for duplex and ferritic stainless steel I-section beam-columns in this subsection. In the calibration of $k_{y,prop}$ and $k_{z,prop}$, the results of the numerical simulations performed on duplex and ferritic stainless steel I-section beam-columns with cross-sections having aspect ratios of $h/b = 1.0$ and 3.0 and falling into Class 1 and Class 3 categories according to EN 1993-1-4 [9] were considered. Stainless steel beam-columns were first subjected to axial compression N_{Ed} resulting in seven different axial loading ratios $n = N_{Ed}/N_{b,Rd}$ ranging between 0.2 and 0.8 in increments of 0.1 and then subjected to increasing bending moments until failure while the axial compression was kept constant. Note that the flange and web

plates of the cross-sections had the same plate buckling slendernesses $\overline{\lambda}_{p,f}$ and $\overline{\lambda}_{p,w}$ under axial compression. For each cross-section and load ratio $n = N_{Ed}/N_{b,Rd}$, the lengths of the beam-columns were selected such that the non-dimensional flexural buckling slenderness $\overline{\lambda}$ of the beam-columns ranged between 0.4 and 2.0 in increments of 0.4. Two additional lengths corresponding to $\overline{\lambda} = 0.2$ and $\overline{\lambda} = 1.0$ were also taken into consideration for each cross-section. In line with [28, 27], the following expression was used to derive the numerical interaction factors k_{FE} from the numerical simulations by rearranging eq. (17) and eq. (18):

$$k_{FE} = \left(1 - \frac{N_{Ed}}{N_{b,Rd}}\right) \frac{M_{csm}}{M_{u,FE}}, \tag{23}$$

where $M_{u,FE}$ is the ultimate bending moment resistance determined through the GMNIA of the beam-columns.

Using the numerically derived interaction factors k_{FE}, the interaction factors k_{prop} are calibrated as shown in Fig. 13. In line with the approach adopted in [28, 25], the maximum values of the k_{FE} factors for each non-dimensional slenderness $\overline{\lambda}$ and axial load ratio $n = N_{Ed}/N_{b,Rd}$ were considered. In the calibration of k_{prop}, the conventional bilinear relationship [31, 30, 27], expressing k_{prop} as a function of the non-dimensional slenderness $\overline{\lambda}$ and load ratio $n = N_{Ed}/N_{b,Rd}$ was employed:

$$k_{prop} = 1 + D_1 \left(\overline{\lambda} - D_2\right) \leq 1 + D_1 \left(D_3 - D_2\right), \tag{24}$$

in which D_1, D_2 and D_3 are coefficients that enable the definition of k_{prop} as a linear function of $\overline{\lambda}$ for the non-dimensional slenderness values less than D_3 (i.e. $\overline{\lambda} < D_3$); while for $\overline{\lambda} \geq D_3$, k_{prop} assumes an upper bound value and remains constant. The D_1 and D_2 coefficients were determined through a regression fit of eq. (24) to the corresponding upper limit numerical interaction factors k_{FE} over the slenderness range between 0.2 and 1.0. The average values of the D_1 and D_2 factors determined considering all load levels $n = N_{Ed}/N_{b,Rd}$ are provided

in Table 8 for duplex and ferritic stainless steel I-section columns under major axis bending and axial compression and minor axis bending and axial compression. In the calibration of the D_3 coefficients, eq. (24) was fitted to the upper limits of $k_{y,FE}$ for low axial compression ratios $n \leq 0.4$ in line with [27]; the calibrated values of D_3 are also provided in Table 8. Using the calibrated D_1, D_2 and D_3 values, the proposed interaction factor expressions k_{prop} are also given in the EN 1993-1-1 [31] format in Table 9.

Comparisons of the numerical k_{FE} and calibrated k_{prop} interaction factors are presented in Fig. 13 where large differences between the k_{FE} and k_{prop} values for high axial compression ratios n and high non-dimensional slendnernesses $\overline{\lambda}$ can be observed. However, these large differences have only a very small influence on the accuracy of the proposed beam-column design method because for beam-columns with high slenderness $\overline{\lambda}$ and high axial loading ratios n, the response is dominated by column buckling and the contribution of the bending term is minimal. Similar observations were also made in [30, 27]. In the following section, the accuracy of the proposed beam-column design method for duplex and ferritic stainless steel I-section beam-columns is assessed.

4.4. Assessment of proposed design rules

An assessment of the accuracy of the proposed design method for duplex and ferritic stainless steel I-section beam-columns is presented in Fig. 14, utilising the results from the extensive numerical parametric studies described in Section 2.6. As can be seen from the figure, the proposed beam-column design approach leads to accurate and safe-sided ultimate strength predictions for duplex and ferritic stainless steel I-section beam-columns for different member slendernesses $\overline{\lambda}$, loading conditions and cross-section properties. A statistical assessment of the accuracy of the proposed design method is also provided in Tables 10 and 11 for duplex and ferritic stainless steel beam-columns, respectively. Comparison of Tables 10 and 11 with Tables 5 and 6 shows that the proposed design method results in ϵ_{COV} values that are lower than those achieved through EN 1993-1-4 [9], AISC Design Guide 27 [10]

and Greiner and Kettler [30], thus indicating that the proposed design rules lead to more consistent ultimate strength predictions relative existing methods. Moreover, the ϵ_{av} values for the proposed method are closer to 1.0 which signifies that the proposed design approach is more accurate relative to the design methods given in [9, 10, 30].

It should be noted that the use of the major and minor axis bending moment resistances determined according to the CSM $M_{y,csm,Rk}$ and $M_{z,csm,Rk}$ in lieu of using the major and minor axis cross-section bending moment resistances $M_{y,c,Rk}$ and $M_{z,c,Rk}$ determined according to the existing rules of EN 1993-1-4 [9] in the application of the proposed design rules has a greater beneficial influence on the predictions of the ultimate resistances of beam-columns with stocky cross-sections and subjected to predominantly bending moments (i.e. beam-columns with stocky sections and low θ values). The greater accuracy of the proposed beam-column design rules also relates to the improved column buckling curves established in [29] particularly for the beam-columns with high levels of axial load; an extensive assessment of the column buckling curves is presented in [29]. Note that since the major and minor axis cross-section bending moment resistance values $M_{c,y,Rk}$ and $M_{c,z,Rk}$ determined according to EN 1993-1-4 [9] are typically lower than the $M_{y,csm,Rk}$ and $M_{z,csm,Rk}$ values calculated according to the CSM, the proposed interaction factors and interaction equations can also be used with the EN 1993-1-4 [9] bending moment end points. An assessment of the resistance predictions obtained using the proposed beam-column interaction equations provided in eqs. (17) and (18) with the EN 1993-1-4 [9] end points $N_{u,prop,EC3}$ is illustrated in Fig. 15. As can be seen from the figure, the proposed beam-column interaction equations also lead to improved accuracy and safety relative to the existing interaction curve when applied with the existing EN 1993-1-4 [9] column strength and cross-section bending moment resistance functions. In the following section, the reliability of the proposed design rules is assessed.

5. Reliability analysis

The reliability of the proposed method for the design of duplex and ferritic stainless steel I-section beam-columns is assessed in this section following the procedure given in Annex D of EN 1990 [49], using the experimental results from [17] and the numerical results obtained through GMNIA in this study. Table 12 shows the key parameters from the reliability analysis, where N is the number of experimental and numerical data points considered, b is the mean value correction factor, $k_{d,n}$ is the fractile factor dependent on the considered number of test and FE results, V_δ is the coefficient of variation of the experimentally and numerically determined ultimate strengths relative to the resistance prediction and γ^*_{M1} is the required value of the partial safety factor. It is worth noting that the mean correction factor b was determined herein by taking the average of the ratios of the experimentally and numerically determined ultimate resistances to those determined through the proposed design method; unlike the least squares approach provided in EN 1990 [49], this prevents the bias of b towards the experimental or numerical results with larger ultimate resistances [50]. In accordance with the recommendations provided in [50], the material overstrength factors, defined as the ratio of the mean yield strength $f_{y,mean}$ to the nominal yield strength $f_{y,nom}$, were taken as $f_{y,mean}/f_{y,nom} = 1.10$ for duplex stainless steel and $f_{y,mean}/f_{y,nom} = 1.20$ for ferritic stainless steel. Moreover, the coefficient of variation of the geometry $V_{geometry}$ was taken as 0.05 (i.e. $V_{geometry} = 0.05$), while the coefficients of variation of the yield strength V_{fy} were taken as 0.03 and 0.045 for duplex and ferritic stainless steel respectively in line with the recommendations provided in [50] (i.e. $V_{fy} = 0.03$ for duplex stainless steel and $V_{fy} = 0.045$ for ferritic stainless steel). As can be seen from Table 12, the required partial safety factors γ^*_{M1} determined for the proposed method are lower than or very close to the partial safety factor value of $\gamma_{M1} = 1.10$ recommended in EN 1993-1-4 [9] and within the limits set out in [51], which indicates that the proposed design method can be safely employed for the design of duplex and ferritic stainless steel I-section beam-columns. It should be noted that

the proposed beam-column design rules also lead to accurate and reliable ultimate strength predictions when applied using the cross-section bending moment resistances determined according to EN 1993-1-4 [9] which do not account for strain hardening in duplex and ferritic stainless steel I-section beam-columns.

6. Conclusions

The behaviour and design of duplex and ferritic stainless steel I-section beam-columns have been explored in this paper. Finite element models able to mimic the structural response of welded duplex and ferritic stainless steel I-section beam-columns were created and validated against experimental results from the literature. The validated models were used to perform Geometrically and Materially Nonlinear Analyses with Imperfections (GMNIA) considering a range of geometries and loading conditions. The results were utilised to assess the accuracy of the beam-column design methods provided in the European structural stainless steel design standard EN 1993-1-4 [9], the American Institute of Steel Construction (AISC) Design Guide 27 [10] and by Greiner and Kettler [30]. It was observed that there is room for improvement in the accuracy of these design methods; hence new beam-column design rules were proposed. The new expressions were shown to provide more accurate and more consistent resistance predictions than existing methods for the design of duplex and ferritic stainless steel beam-columns. The reliability of the proposals, which are recommended for inclusion in future revisions of Eurocode 3: Part 1.4, was verified in accordance with Annex D of EN 1990 [49]. Future research will focus on the flexural-torsional buckling response and design of laterally-unrestrained duplex and ferritic stainless steel I-section beam-columns, including those with Class 4 cross-sections, where local-global interactive buckling is anticipated.

References

[1] Gardner, L., Nethercot, D.A.. Experiments on stainless steel hollow sections—Part 1: Material and cross-sectional behaviour. Journal of Constructional Steel Research 2004;60(9):1291–1318.

[2] Gardner, L., Nethercot, D.A.. Experiments on stainless steel hollow sections—Part 2: Member behaviour of columns and beams. Journal of Constructional Steel Research 2004;60(9):1319–1332.

[3] Young, B., Lui, W.M.. Behavior of cold-formed high strength stainless steel sections. Journal of Structural Engineering, ASCE 2005;131(11):1738–1745.

[4] Becque, J., Rasmussen, K.J.. Experimental investigation of local-overall interaction buckling of stainless steel lipped channel columns. Journal of Constructional Steel Research 2009;65(8-9):1677–1684.

[5] Rossi, B., Jaspart, J.P., Rasmussen, K.J.. Combined distortional and overall flexural-torsional buckling of cold-formed stainless steel sections: Experimental investigations. Journal of Structural Engineering, ASCE 2009;136(4):354–360.

[6] Huang, Y., Young, B.. Experimental and numerical investigation of cold-formed lean duplex stainless steel flexural members. Thin-Walled Structures 2013;73:216–228.

[7] Huang, Y., Young, B.. Experimental investigation of cold-formed lean duplex stainless steel beam-columns. Thin-Walled Structures 2014;76:105–117.

[8] Gardner, L.. Stability and design of stainless steel structures–Review and outlook. Thin-Walled Structures 2019;141:208–216.

[9] EN 1993-1-4, Eurocode 3 Design of steel structures-Part 1-4: General rules – Supplementary rules for stainless steel. European Committee for Standardization (CEN), Brussels; 2015.

[10] AISC Design Guide 27: Structural Stainless Steel. American Institute of Steel Construction (AISC), Chicago, Illinois, USA; 2013.

[11] AS/NZS 4673, Cold-formed stainless steel structures. Australian/New Zealand Standard, Sydney; 2001.

[12] SEI/ASCE 8-02, Specification for the design of cold-formed stainless steel structural members. American Society of Civil Engineers (ASCE), Reston; 2002.

[13] Burgan, B., Baddoo, N., Gilsenan, K.. Structural design of stainless steel members—Comparison between Eurocode 3, Part 1.4 and test results. Journal of Constructional Steel Research 2000;54(1):51–73.

[14] Zheng, B., Hua, X., Shu, G.. Tests of cold-formed and welded stainless steel beam-columns. Journal of Constructional Steel Research 2015;111:1–10.

[15] Ahmed, S., Al-Deen, S., Ashraf, M.. Design rules for stainless steel welded I-columns based on experimental and numerical studies. Engineering Structures 2018;172:850–868.

[16] Yang, L., Zhao, M., Chan, T.M., Shang, F., Xu, D.. Flexural buckling of welded austenitic and duplex stainless steel I-section columns. Journal of Constructional Steel Research 2016;122:339–353.

[17] Yang, L., Zhao, M., Gardner, L., Ning, K., Wang, J.. Member stability of stainless steel welded I-section beam-columns. Journal of Constructional Steel Research 2019;155:33–45.

[18] Yuan, H., Wang, Y., Shi, Y., Gardner, L.. Residual stress distributions in welded stainless steel sections. Thin-Walled Structures 2014;79:38–51.

[19] Bredenkamp, P., Van den Berg, G.. The strength of stainless steel built-up I-section columns. Journal of Constructional Steel Research 1995;34(2-3):131–144.

[20] Yang, L., Wang, Y., Gao, B., Shi, Y., Yuan, H.. Two calculation methods for buckling reduction factors of stainless steel welded I-section beams. Thin-Walled Structures 2014;83:128–136.

[21] Wang, Y., Yang, L., Gao, B., Shi, Y., Yuan, H.. Experimental study of lateral-torsional buckling behavior of stainless steel welded I-section beams. International Journal of Steel Structures 2014;14(2):411–420.

[22] Saliba, N., Gardner, L.. Cross-section stability of lean duplex stainless steel welded I-sections. Journal of Constructional Steel Research 2013;80:1–14.

[23] Yuan, H., Wang, Y., Shi, Y., Gardner, L.. Stub column tests on stainless steel built-up sections. Thin-Walled Structures 2014;83:103–114.

[24] Gardner, L., Bu, Y., Theofanous, M.. Laser-welded stainless steel I-sections: Residual stress measurements and column buckling tests. Engineering Structures 2016;127:536–548.

[25] Bu, Y., Gardner, L.. Finite element modelling and design of welded stainless steel I-section columns. Journal of Constructional Steel Research 2019;152:57–67.

[26] Bu, Y., Gardner, L.. Local stability of laser-welded stainless steel I-sections in bending. Journal of Constructional Steel Research 2018;148:49–64.

[27] Bu, Y., Gardner, L.. Laser-welded stainless steel I-section beam-columns: Testing, simulation and design. Engineering Structures 2019;179:23–36.

[28] Kucukler, M., Gardner, L., Bu, Y.. Flexural-torsional buckling of austenitic stainless steel I-section beam-columns: Testing, numerical modelling and design. Thin-Walled Structures 2020;152:106572.

[29] Kucukler, M.. Flexural buckling behaviour and design of duplex and ferritic stainless steel I-section columns. Thin-Walled Structures 2020;156:106953.

[30] Greiner, R., Kettler, M.. Interaction of bending and axial compression of stainless steel members. Journal of Constructional Steel Research 2008;64(11):1217–1224.

[31] EN 1993-1-1, Eurocode 3 Design of steel structures-Part 1-1: General rules and rules for buildings. European Committee for Standardization (CEN), Brussels; 2005.

[32] Abaqus 2018 Reference Manual. Simulia, Dassault Systemes; 2018.

[33] Kucukler, M., Gardner, L., Macorini, L.. Lateral–torsional buckling assessment of steel beams through a stiffness reduction method. Journal of Constructional Steel Research 2015;109:87–100.

[34] Kucukler, M., Gardner, L., Macorini, L.. Flexural–torsional buckling assessment of steel beam–columns through a stiffness reduction method. Engineering Structures 2015;101:662–676.

[35] Kucukler, M., Gardner, L.. Design of web-tapered steel beams against lateral-torsional buckling through a stiffness reduction method. Engineering Structures 2019;190:246–261.

[36] Kucukler, M.. Lateral instability of steel beams in fire: Behaviour, numerical modelling and design. Journal of Constructional Steel Research 2020;170:106095.

[37] Kucukler, M.. Compressive resistance of high-strength and normal-strength steel CHS members at elevated temperatures. Thin-Walled Structures 2020;152:106753.

[38] Mirambell, E., Real, E.. On the calculation of deflections in structural stainless steel beams: an experimental and numerical investigation. Journal of Constructional Steel Research 2000;54(1):109–133.

[39] Arrayago, I., Real, E., Gardner, L.. Description of stress–strain curves for stainless steel alloys. Materials & Design 2015;87:540–552.

[40] Afshan, S., Zhao, O., Gardner, L.. Standardised material properties for numerical parametric studies of stainless steel structures and buckling curves for tubular columns. Journal of Constructional Steel Research 2019;152:2–11.

[41] EN 1990-2, Execution of Steel Structures and Aluminium Structures-Part 2: Technical Requirements for Steel Structures. European Committee for Standardization (CEN), Brussels; 2008.

[42] EN 1993-1-2, Eurocode 3 Design of steel structures-Part 1-2: General rules – Structural fire design. European Committee for Standardization (CEN), Brussels; 2005.

[43] Martins, J., da Silva, L.S., Tankova, T., Craveiro, H.. Reliability assessment of EC3-1-5 methodology of welded slender cross-sections under direct stresses. Journal of Constructional Steel Research 2019;160:301–319.

[44] Le, T., Bradford, M.A., Liu, X., Valipour, H.R.. Buckling of welded high-strength steel i-beams.

Journal of Constructional Steel Research 2020;168:105938.

[45] Jandera, M., Gardner, L., Machacek, J.. Residual stresses in cold-rolled stainless steel hollow sections. Journal of Constructional Steel Research 2008;64(11):1255–1263.

[46] Afshan, S., Gardner, L.. The continuous strength method for structural stainless steel design. Thin-Walled Structures 2013;68:42–49.

[47] Gardner, L., Wang, F., Liew, A.. Influence of strain hardening on the behavior and design of steel structures. International Journal of Structural Stability and Dynamics 2011;11(05):855–875.

[48] Walport, F., Gardner, L., Nethercot, D.. Design of structural stainless steel members by second order inelastic analysis with CSM strain limits. Thin-Walled Structures 2021;159:107267.

[49] EN 1990, Basis for structural design. European Committee for Standardization (CEN), Brussels; 2005.

[50] Afshan, S., Francis, P., Baddoo, N., Gardner, L.. Reliability analysis of structural stainless steel design provisions. Journal of Constructional Steel Research 2015;114:293–304.

[51] da Silva, L.S., Marques, L., Tankova, T., Rebelo, C., Kuhlmann, U., Kleiner, A., et al. SAFEBRICTILE: Standardization of safety assessment procedures across brittle to ductile failure modes. Research programme of Research Fund for Coal & Steel, Final report; 2017.

Figures captions

Figure 1 : Two-stage compound Ramberg-Osgood material model and stress-strain response of duplex and ferritic stainless steel employed in this study

Figure 2 : Global and local buckling modes used to model geometric imperfections for beam-columns under combined major axis bending and axial compression

Figure 3 : Global and local buckling modes used to model geometric imperfections for beam-columns under combined minor axis bending and axial compression

Figure 4 : Membrane (i.e. constant through thickness) residual stress pattern adopted for welded stainless steel I-sections (+ve = tension, -ve = compression)

Figure 5 : Comparison of load versus mid-height displacement paths obtained through the finite models and those observed in the experiments of [17] for beam-column specimens subjected to major axis bending plus axial compression

Figure 6 : Comparison of load versus mid-height displacement paths obtained through the finite models and those observed in the experiments of [17] for the beam-column specimens subjected to minor axis bending plus axial compression

Figure 7 : Comparisons of experimental [17] and numerical failure modes for specimen I 304-2500, with stresses in MPa

Figure 8 : Comparisons of experimental [17] and numerical failure modes for specimen

H 304-2500, with stresses in MPa

Figure 9 : Method adopted for the assessment of the accuracy of different design methods against the results obtained from finite element (FE) models and physical tests

Figure 10 : Assessment of accuracy of EN 1993-1-4 [9] for duplex and ferritic stainless steel I-section beam-columns under combined major axis bending and compression and combined minor axis bending and compression

Figure 11 : Assessment of accuracy of AISC Design Guide 27 [10] for duplex and ferritic stainless steel I-section beam-columns under combined major axis bending and compression and combined minor axis bending and compression

Figure 12 : Assessment of accuracy of the beam-column design method of Greiner and Kettler [30] for duplex and ferritic stainless steel I-section beam-columns under combined major axis bending and compression and combined minor axis bending and compression

Figure 13 : Calibration of interaction factors $k_{y,prop}$ and $k_{z,prop}$ for duplex and ferritic stainless steel I-section beam-columns

Figure 14 : Assessment of accuracy of proposed design method for duplex and ferritic stainless steel I-section beam-columns

Figure 15 : Assessment of accuracy of proposed beam-column interaction equations for duplex and ferritic stainless steel I-section beam-columns when they are used in conjunction with column curves and bending moment cross-section strength equations provided in EN

1993-1-4 [9]

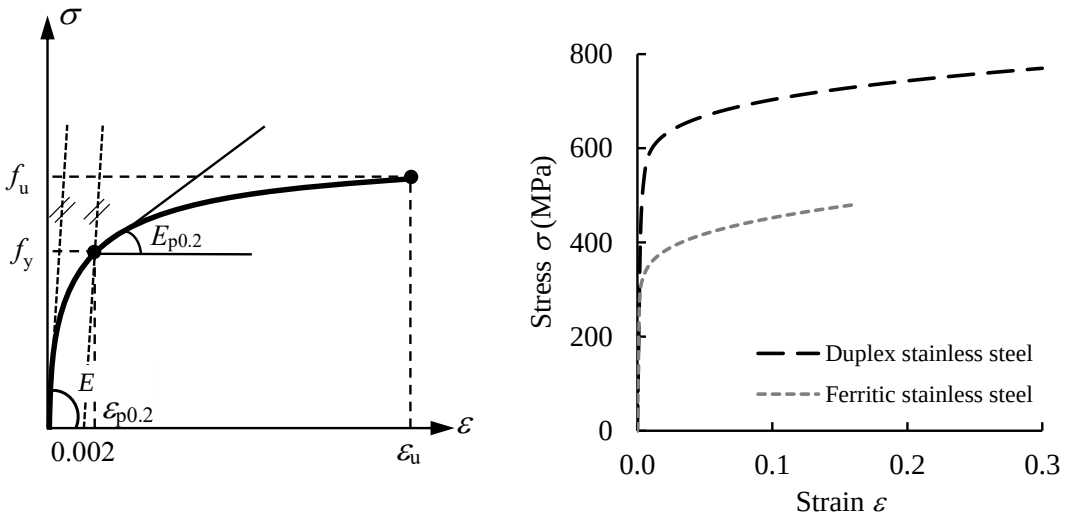

(a) Material model (b) Stress-strain curves

Figure 1: Two-stage compound Ramberg-Osgood material model and stress-strain response of duplex and ferritic stainless steel employed in this study

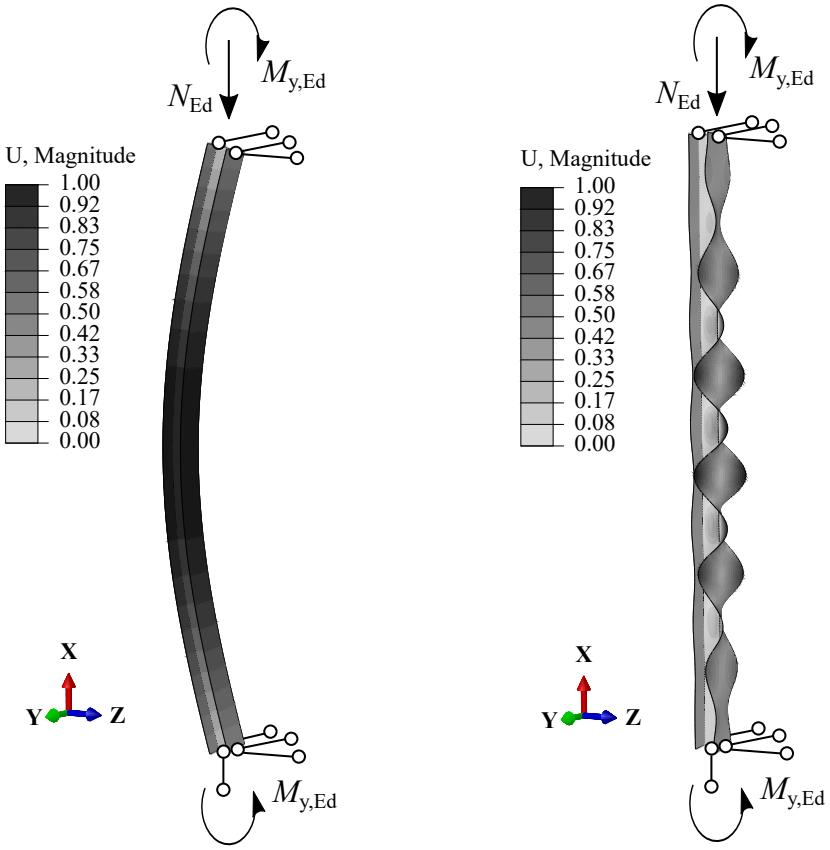

(a) Global buckling mode (b) Local buckling mode

Figure 2: Global and local buckling modes used to model geometric imperfections for beam-columns under combined major axis bending and axial compression

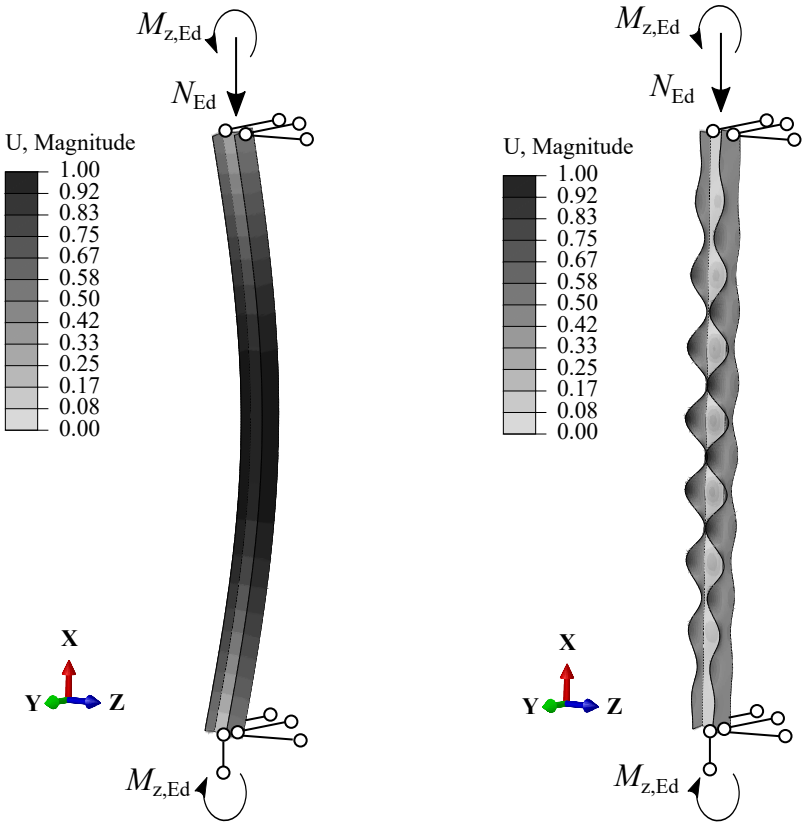

(a) Global buckling mode (b) Local buckling mode

Figure 3: Global and local buckling modes used to model geometric imperfections for beam-columns under combined minor axis bending and axial compression

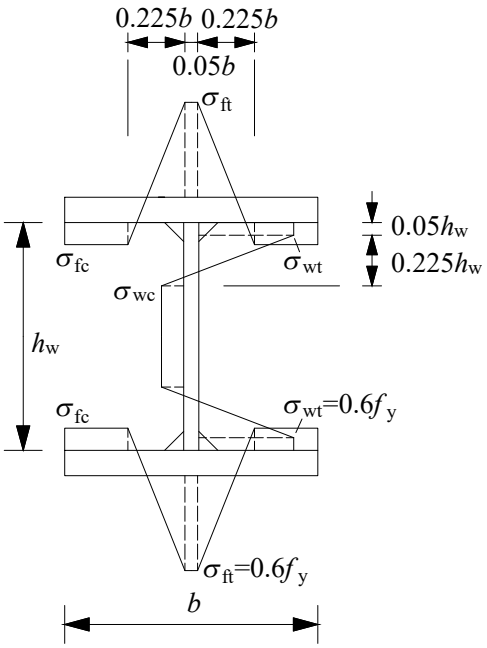

Figure 4: Membrane (i.e. constant through thickness) residual stress pattern adopted for welded stainless steel I-sections (+ve = tension, -ve = compression)

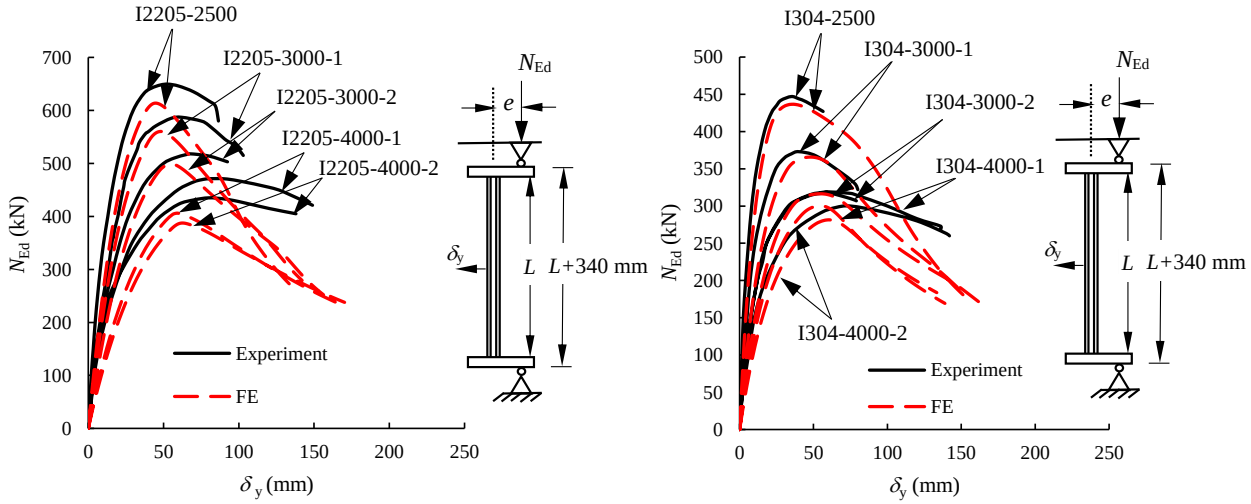

(a) Duplex stainless steel beam-columns

(b) Austenitic stainless steel beam-columns

Figure 5: Comparison of load versus mid-height displacement paths obtained through the finite models and those observed in the experiments of [17] for beam-column specimens subjected to major axis bending plus axial compression

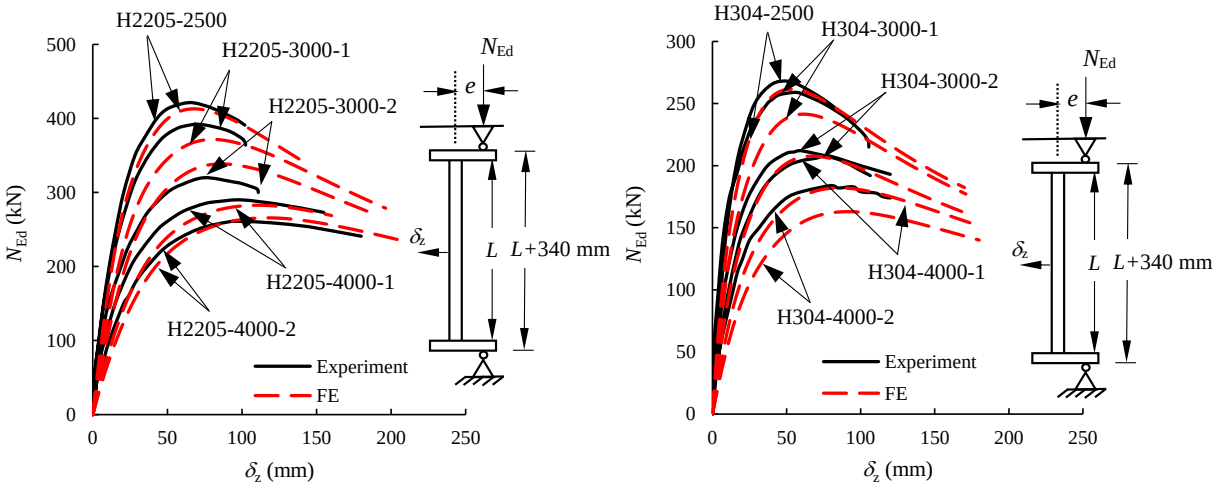

(a) Duplex stainless steel beam-columns (b) Austenitic stainless steel beam-columns

Figure 6: Comparison of load versus mid-height displacement paths obtained through the finite models and those observed in the experiments of [17] for the beam-column specimens subjected to minor axis bending plus axial compression

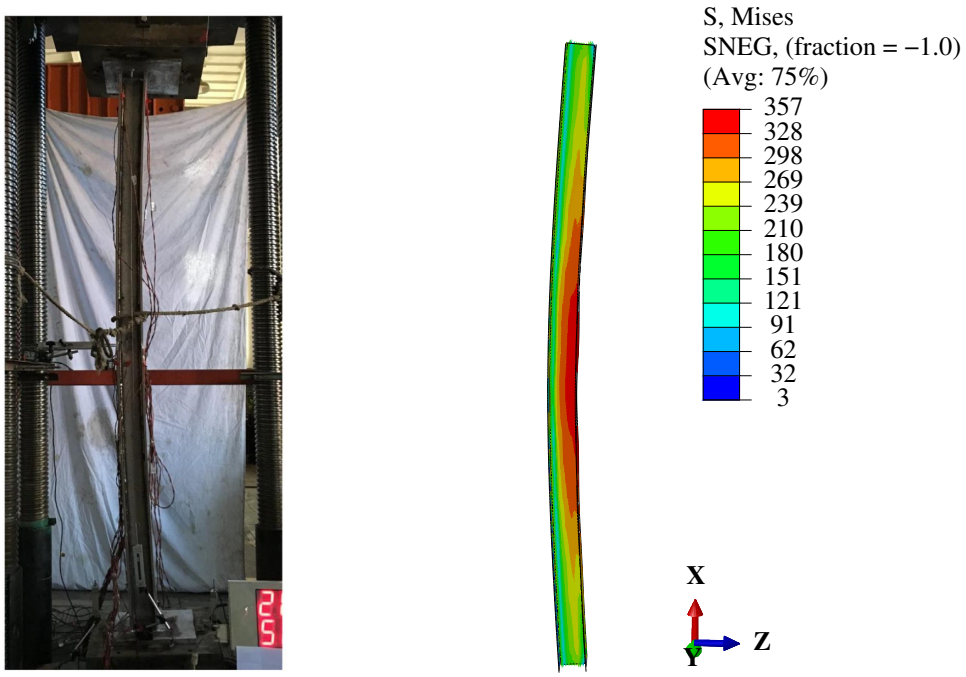

(a) I 304-2500 experiment (b) I 304-2500 FE model

Figure 7: Comparisons of experimental [17] and numerical failure modes for specimen I 304-2500, with stresses in MPa

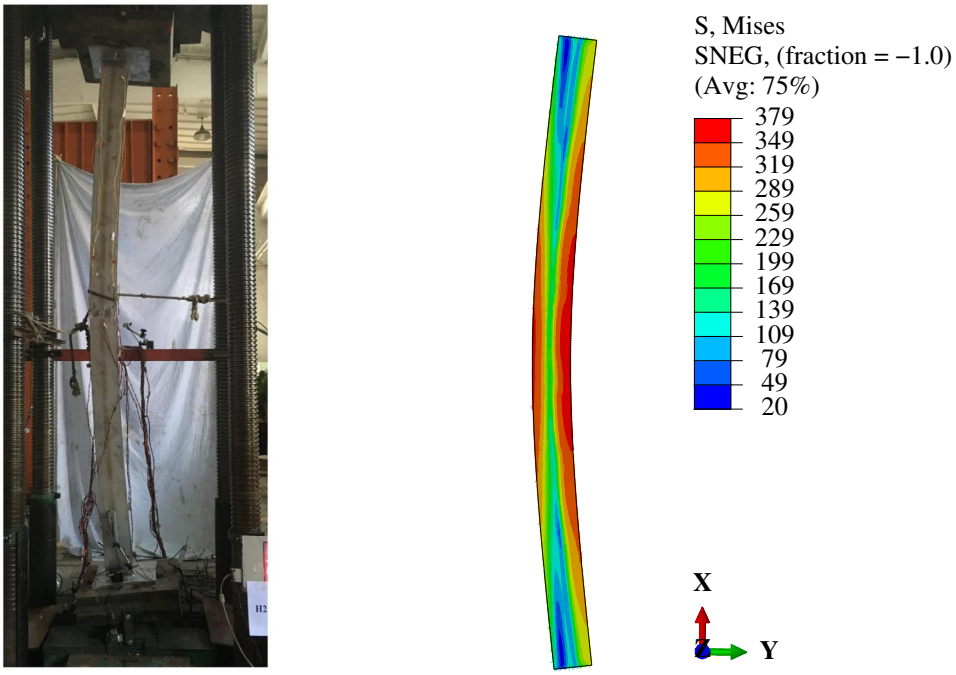

(a) H 304-2500 experiment (b) H 304-2500 FE model

Figure 8: Comparisons of experimental [17] and numerical failure modes for specimen H 304-2500, with stresses in MPa

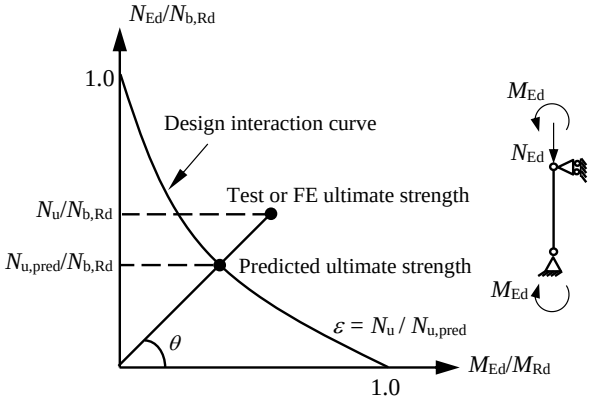

Figure 9: Method adopted for the assessment of the accuracy of different design methods against the results obtained from finite element (FE) models and physical tests

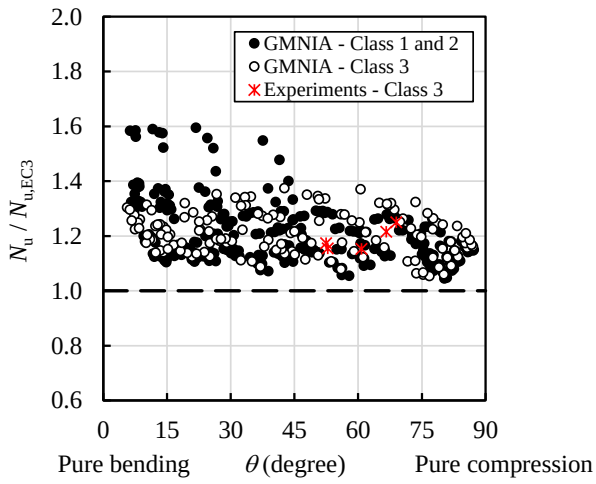

(a) Duplex stainless steel beam-columns – Major axis bending and compression

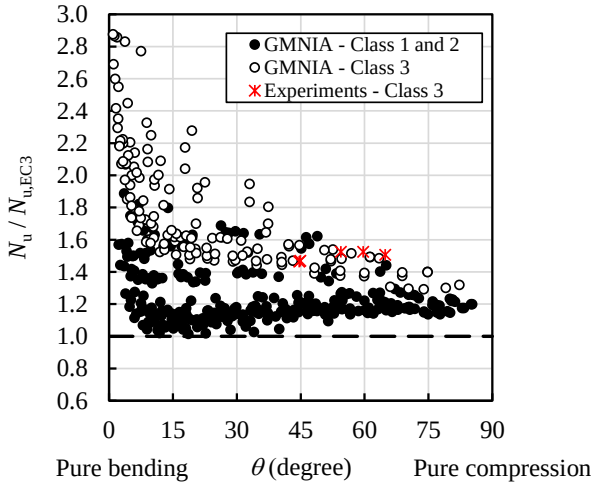

(b) Duplex stainless steel beam-columns – Minor axis bending and compression

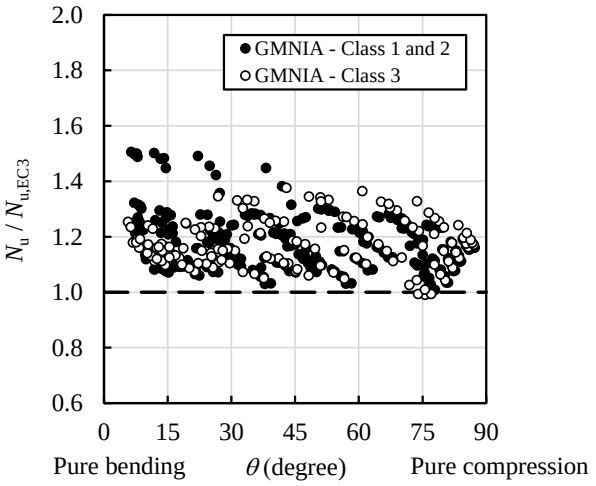

(c) Ferritic stainless steel beam-columns – Major axis bending and compression

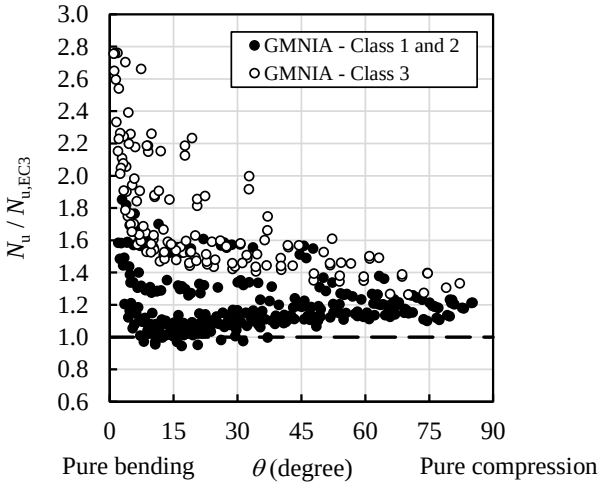

(d) Ferritic stainless steel beam-columns – Minor axis bending and compression

Figure 10: Assessment of accuracy of EN 1993-1-4 [9] for duplex and ferritic stainless steel I-section beam-columns under combined major axis bending and compression and combined minor axis bending and compression

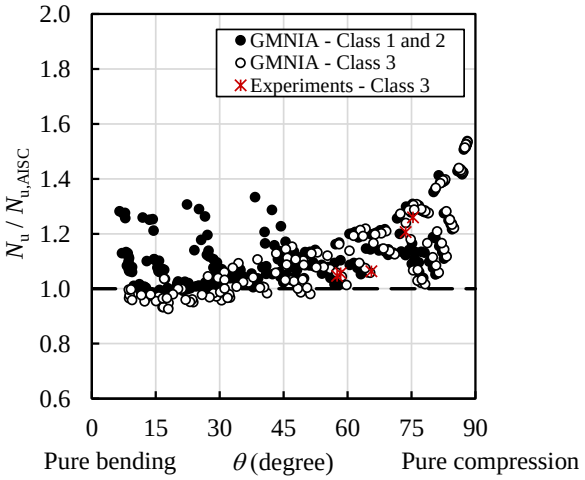

(a) Duplex stainless steel beam-columns – Major axis bending and compression

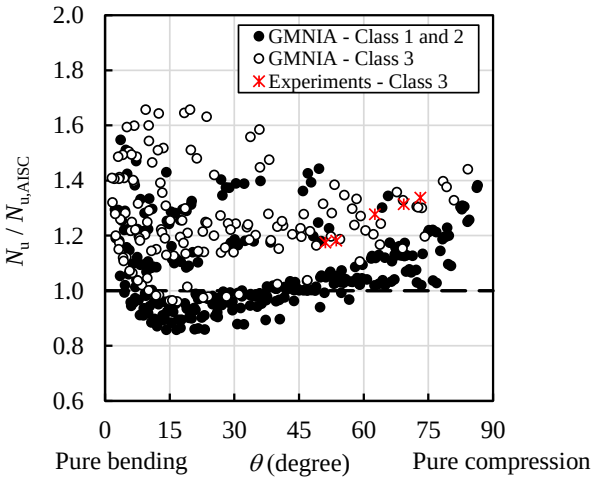

(b) Duplex stainless steel beam-columns – Minor axis bending and compression

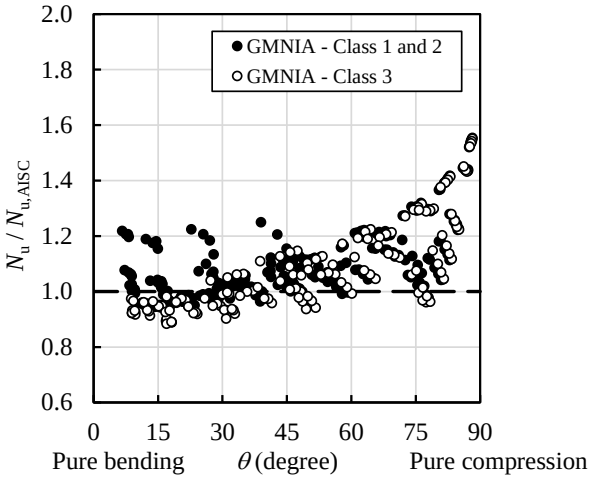

(c) Ferritic stainless steel beam-columns – Major axis bending and compression

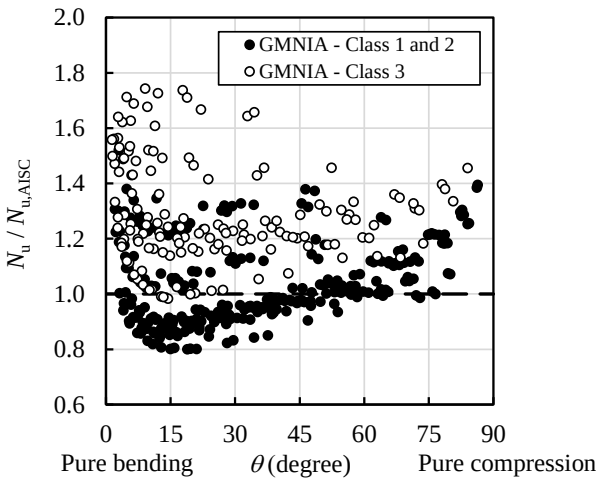

(d) Ferritic stainless steel beam-columns – Minor axis bending and compression

Figure 11: Assessment of accuracy of AISC Design Guide 27 [10] for duplex and ferritic stainless steel I-section beam-columns under combined major axis bending and compression and combined minor axis bending and compression

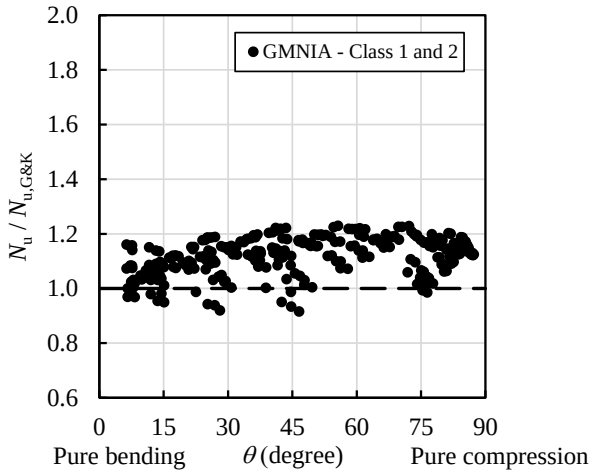

(a) Duplex stainless steel beam-columns – Major axis bending and compression

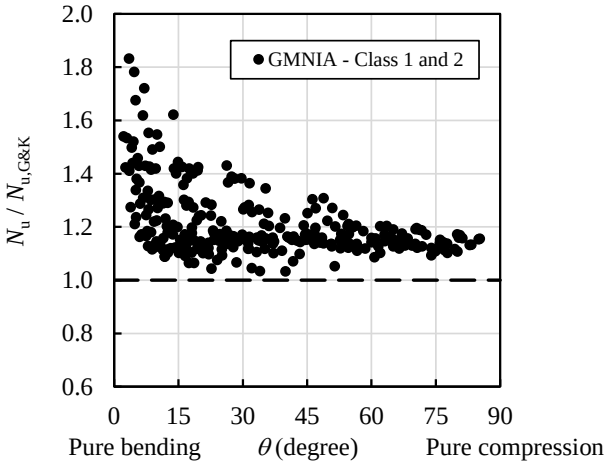

(b) Duplex stainless steel beam-columns – Minor axis bending and compression

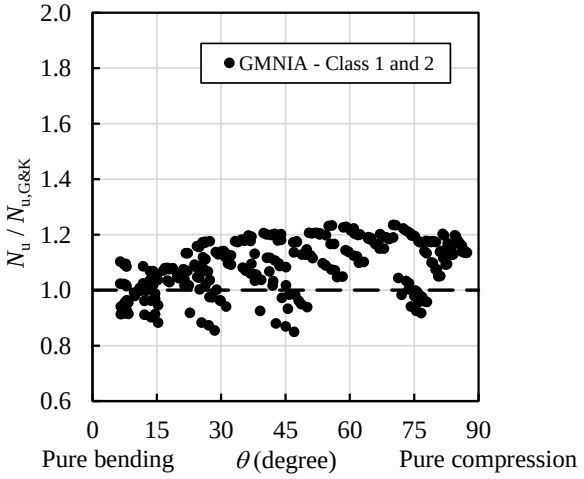

(c) Ferritic stainless steel beam-columns – Major axis bending and compression

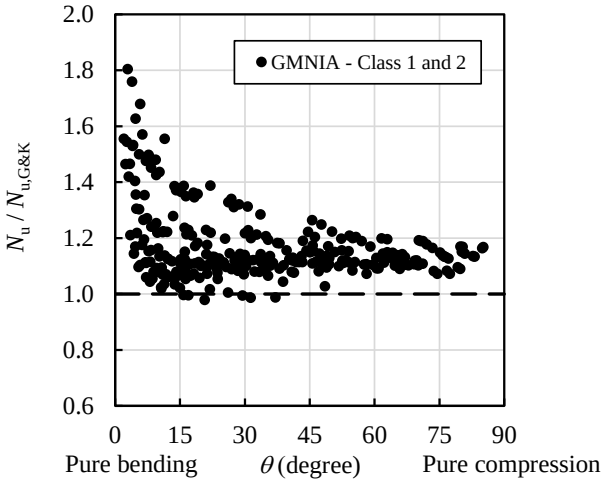

(d) Ferritic stainless steel beam-columns – Minor axis bending and compression

Figure 12: Assessment of accuracy of the beam-column design method of Greiner and Kettler [30] for duplex and ferritic stainless steel I-section beam-columns under combined major axis bending and compression and combined minor axis bending and compression

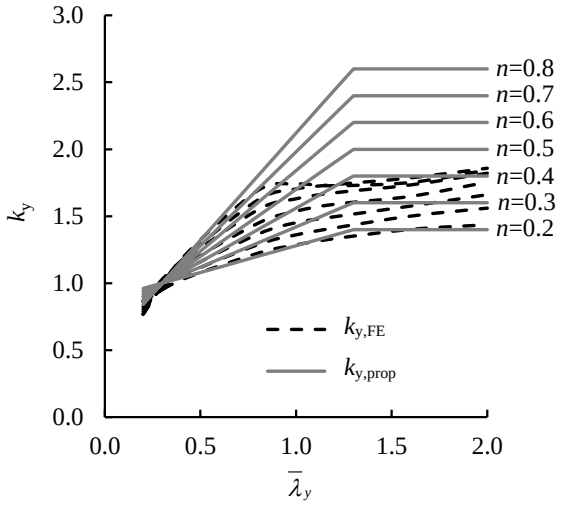

(a) Duplex beam-columns under major axis bending and compression

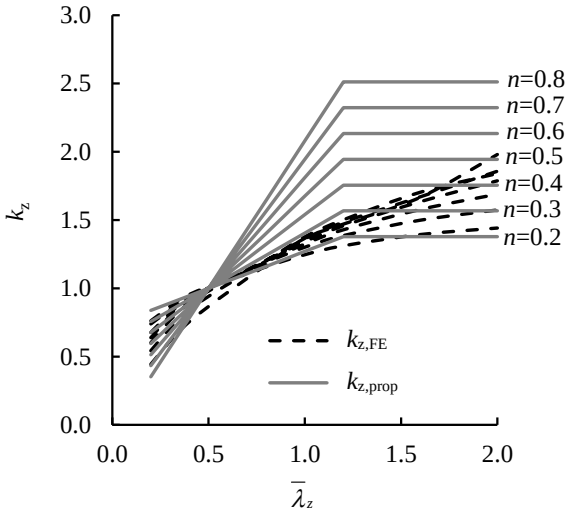

(b) Duplex beam-columns under minor axis bending and compression

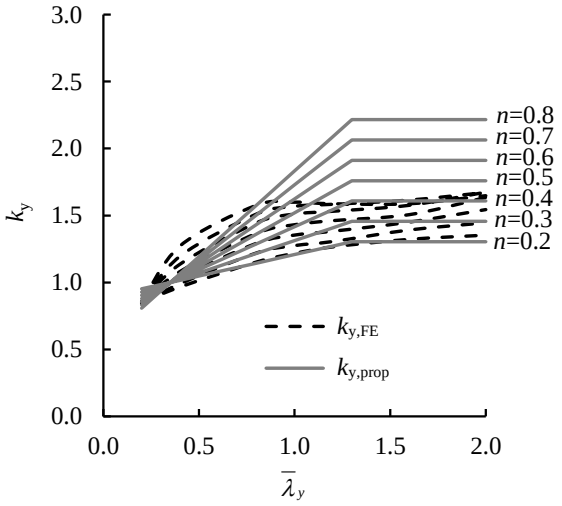

(c) Ferritic beam-columns under major axis bending and compression

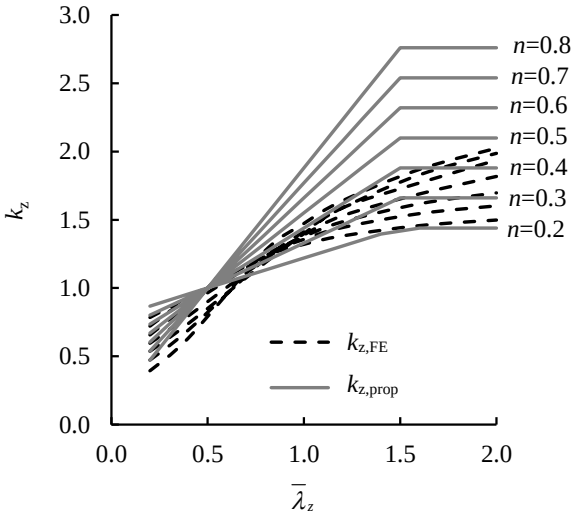

(d) Ferritic beam-columns under minor axis bending and compression

Figure 13: Calibration of interaction factors $k_{y,prop}$ and $k_{z,prop}$ for duplex and ferritic stainless steel I-section beam-columns

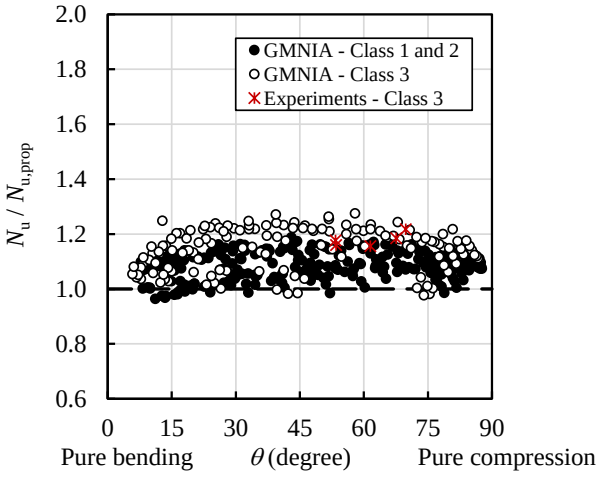

(a) Duplex stainless steel beam-columns – Major axis bending and compression

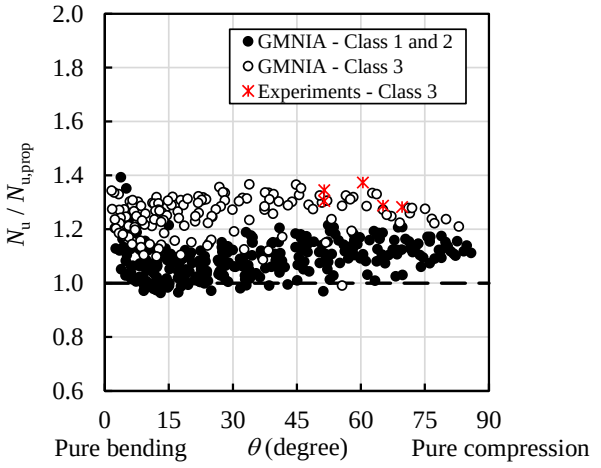

(b) Duplex stainless steel beam-columns – Minor axis bending and compression

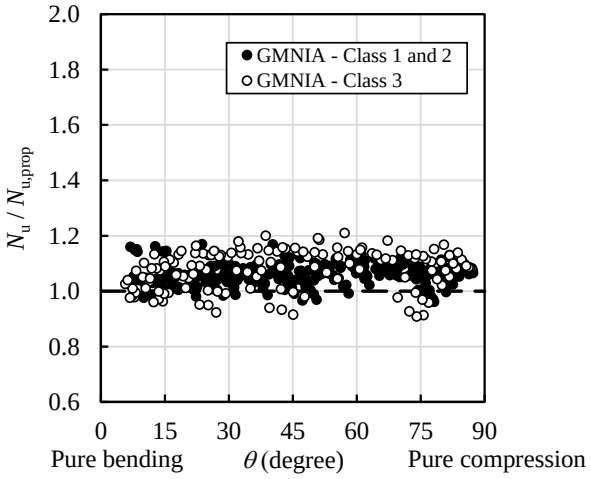

(c) Ferritic stainless steel beam-columns – Major axis bending and compression

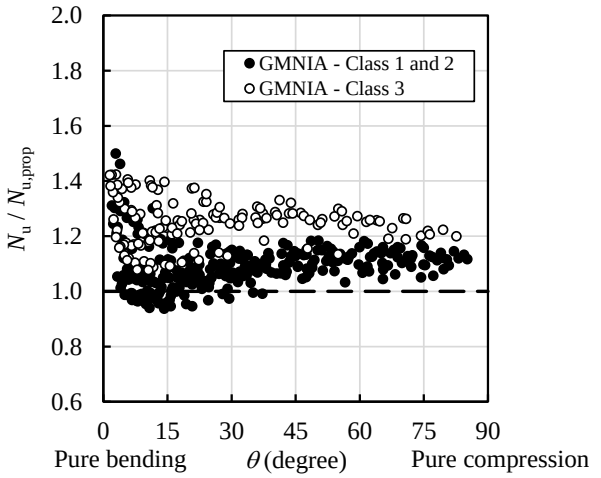

(d) Ferritic stainless steel beam-columns – Minor axis bending and compression

Figure 14: Assessment of accuracy of proposed design method for duplex and ferritic stainless steel I-section beam-columns

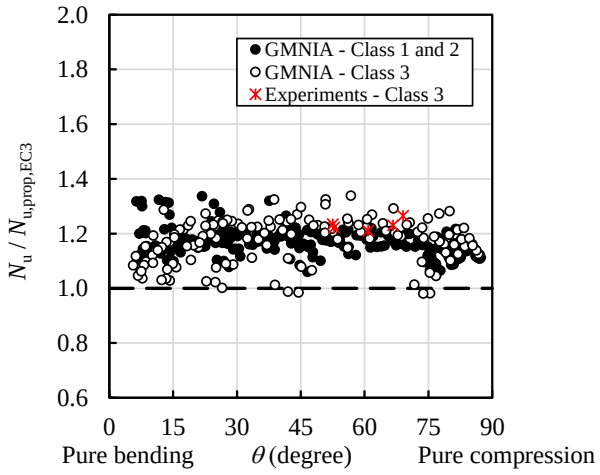

(a) Duplex stainless steel beam-columns – Major axis bending and compression

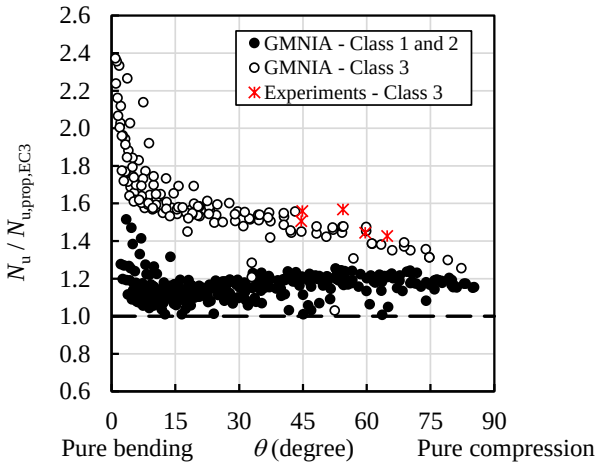

(b) Duplex stainless steel beam-columns – Minor axis bending and compression

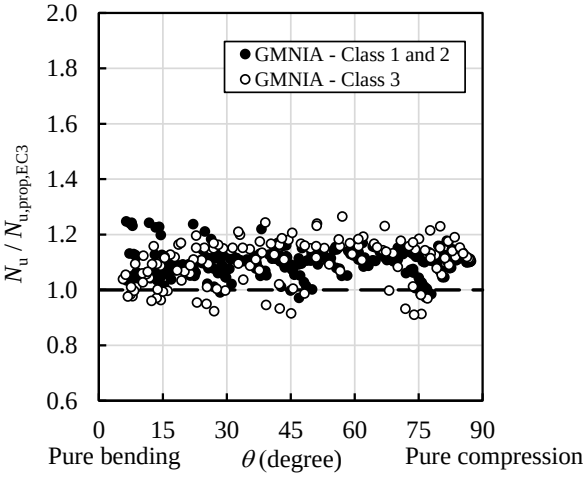

(c) Ferritic stainless steel beam-columns – Major axis bending and compression

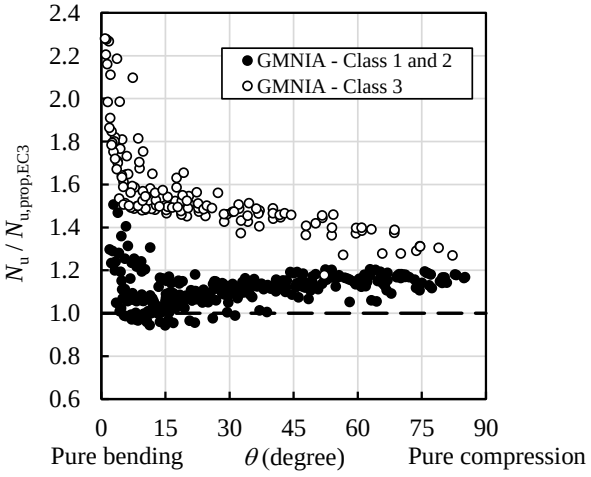

(d) Ferritic stainless steel beam-columns – Minor axis bending and compression

Figure 15: Assessment of accuracy of proposed beam-column interaction equations for duplex and ferritic stainless steel I-section beam-columns when used in conjunction with column curves and bending moment cross-section strength equations provided in EN 1993-1-4 [9]

Tables captions

Table 1 : Material properties used to define the stress-strain response of duplex and ferritic stainless steel in this study

Table 2 : Comparison of ultimate resistances of stainless steel beam-columns obtained during the experiments of [17] and those determined from the finite element models for beam-columns subjected to major axis bending plus axial compression

Table 3 : Comparison of ultimate resistances of stainless steel beam-columns obtained from the experiments of [17] and those determined from the finite element models or beam-columns subjected to minor axis bending plus axial compression

Table 4 : Summary of numerical parametric studies performed

Table 5 : Assessment of accuracy of existing design methods for duplex stainless steel welded I-section beam-columns

Table 6 : Assessment of accuracy of existing design methods for ferritic stainless steel welded I-section beam-columns

Table 7 : Imperfection factor α and threshold slenderness $\overline{\lambda}_0$ values proposed in Kucukler [28] for duplex and ferritic stainless steel welded I-section columns

Table 8 : Calibrated expressions of $k_{y,prop}$ and $k_{z,prop}$

Table 9 : Assessment of accuracy of proposed design rules for duplex stainless steel welded I-section beam-columns

Table 10 : Assessment of accuracy of proposed design rules for ferritic stainless steel welded I-section beam-columns

Table 11 : Reliability analysis of proposed design method for duplex and ferritic stainless steel welded I-section beam-columns

Table 1: Material properties used to define the stress-strain response of duplex and ferritic stainless steel in this study

Stainless steel grade	f_y (MPa)	f_u (MPa)	ϵ_u	n	m
Duplex	530	770	0.30	9.3	3.6
Ferritic	320	480	0.16	17.2	2.8

Table 2: Comparison of ultimate resistances of stainless steel beam-columns obtained during the experiments of [17] and those determined from the finite element models for beam-columns subjected to major axis bending plus axial compression

Specimen	$\overline{\lambda}_y$	$N_{ult,exp}$ (kN)	$\omega_g = e_{0,m}$		$\omega_g = L/1000$	
			$N_{ult,FE}$ (kN)	$N_{ult,FE}/N_{ult,exp}$	$N_{ult,FE}$ (kN)	$N_{ult,FE}/N_{ult,exp}$
I 2205-2500	0.95	649.5	613.7	0.94	617.9	0.95
I 2205-3000-1	1.11	597.8	560.2	0.94	557.7	0.93
I 2205-3000-2	1.12	516.6	498.9	0.97	487.3	0.94
I 2205-4000-1	1.46	472.4	405.9	0.86	404.2	0.86
I 2205-4000-2	1.46	439.2	387.5	0.88	381.1	0.87
			Average	0.92	Average	0.91
			COV	0.049	COV	0.049
I 304-2500	0.69	454.0	436.6	0.96	445.2	0.98
I 304-3000-1	0.80	376.4	365.7	0.97	371.6	0.99
I 304-3000-2	0.82	321.1	316.4	0.99	308.4	0.96
I 304-4000-1	1.06	324.7	300.2	0.92	289.5	0.89
I 304-4000-2	1.07	306.3	281.4	0.92	273.2	0.89
			Average	0.95	Average	0.94
			COV	0.031	COV	0.050

Table 3: Comparison of ultimate resistances of stainless steel beam-columns obtained from the experiments of [17] and those determined from the finite element models for beam-columns subjected to minor axis bending plus axial compression

Specimen	$\overline{\lambda}_z$	$N_{ult,exp}$ (kN)	$\omega_g = e_{0,m}$		$\omega_g = L/1000$	
			$N_{ult,FE}$ (kN)	$N_{ult,FE}/N_{ult,exp}$	$N_{ult,FE}$ (kN)	$N_{ult,FE}/N_{ult,exp}$
H 2205-2500	1.25	428.1	413.0	0.96	404.1	0.94
H 2205-3000-1	1.47	398.6	371.7	0.93	362.9	0.91
H 2205-3000-2	1.47	324.7	338.6	1.04	320.9	0.99
H 2205-4000-1	1.91	291.5	282.8	0.97	280.4	0.96
H 2205-4000-2	1.90	269.4	265.7	0.99	259.1	0.96
			Average	0.98	Average	0.95
			COV	0.041	COV	0.030
H 304-2500	0.91	269.4	261.5	0.97	254.4	0.94
H 304-3000-1	1.07	262.0	241.5	0.92	239.8	0.92
H 304-3000-2	1.07	217.7	207.7	0.95	206.9	0.95
H 304-4000-1	1.38	210.3	163.0	0.77	183.0	0.87
H 304-4000-2	1.39	188.2	182.1	0.97	176.2	0.94
			Average	0.92	Average	0.92
			COV	0.090	COV	0.035

Table 4: Summary of numerical parametric studies performed

Loading condition	Cross-section aspect ratio h/b	Cross-section class	Stainless steel type	$\overline{\lambda}$
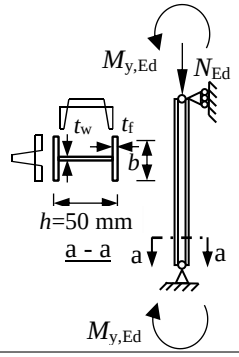	1.0 1.5 2.0 3.0	Class 1 Class 2 Class 3	Duplex Ferritic	0.2 0.4 0.8 1.0 1.2 1.6 2.0
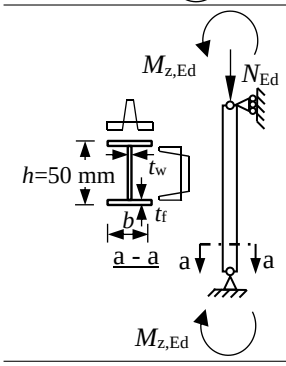	1.0 1.5 2.0 3.0	Class 1 Class 2 Class 3	Duplex Ferritic	0.2 0.4 0.8 1.0 1.2 1.6 2.0

Table 5: Assessment of accuracy of existing design methods for duplex stainless steel welded I-section beam-columns

Design method	Loading	Section class	N	ϵ_{av}	ϵ_{COV}	ϵ_{max}	ϵ_{min}
EN 1993-1-4 [9]	Major axis bending and compression	Class 1 & 2	280	1.21	0.092	1.59	1.04
		Class 3	145	1.21	0.062	1.37	1.05
	Minor axis bending and compression	Class 1 & 2	280	1.25	0.144	1.89	1.01
		Class 3	145	1.77	0.208	2.88	1.29
AISC Design Guide 27 [10]	Major axis bending and compression	Class 1 & 2	280	1.14	0.112	1.54	0.97
		Class 3	145	1.10	0.131	1.53	0.93
	Minor axis bending and compression	Class 1 & 2	280	1.08	0.137	1.55	0.86
		Class 3	145	1.26	0.131	1.66	0.96
Greiner and Kettler [30]	Major axis bending and compression	Class 1 & 2	280	1.12	0.061	1.23	0.91
		Class 3	–	–	–	–	–
	Minor axis bending and compression	Class 1 & 2	280	1.21	0.107	1.83	1.03
		Class 3	–	–	–	–	–

Table 6: Assessment of accuracy of existing design methods for ferritic stainless steel welded I-section beam-columns

Design method	Loading	Section class	N	ϵ_{av}	ϵ_{COV}	ϵ_{max}	ϵ_{min}
EN 1993-1-4 [9]	Major axis bending and compression	Class 1 & 2	280	1.17	0.084	1.50	1.01
		Class 3	140	1.17	0.073	1.38	0.99
	Minor axis bending and compression	Class 1 & 2	280	1.21	0.148	1.85	0.94
		Class 3	140	1.73	0.208	2.76	1.26
AISC Design Guide 27 [10]	Major axis bending and compression	Class 1 & 2	280	1.11	0.129	1.55	0.93
		Class 3	140	1.08	0.150	1.55	0.88
	Minor axis bending and compression	Class 1 & 2	280	1.04	0.146	1.52	0.80
		Class 3	140	1.30	0.144	1.74	0.98
Greiner and Kettler [30]	Major axis bending and compression	Class 1 & 2	280	1.09	0.085	1.23	0.85
		Class 3	–	–	–	–	–
	Minor axis bending and compression	Class 1 & 2	280	1.17	0.113	1.80	0.98
		Class 3	–	–	–	–	–

Table 7: Imperfection factor α and threshold slenderness $\overline{\lambda}_0$ values proposed in Kucukler [28] for duplex and ferritic stainless steel welded I-section columns

Stainless steel type	Axis of buckling	α	$\overline{\lambda}_0$
Duplex	Major	0.49	0.30
	Minor	0.76	0.30
Ferritic	Major	0.42	0.20
	Minor	0.64	0.20

Table 8: Calibrated D_1, D_2 and D_3 coefficients for the determination of interaction factors k_{prop}

Loading conditions	Stainless steel type	D_1	D_2	D_3
Compression plus major axis bending $k_{y,prop}$	Duplex	2.0	0.3	1.3
	Ferritic	1.6	0.35	1.3
Compression plus minor axis bending $k_{z,prop}$	Duplex	2.7	0.5	1.2
	Ferritic	2.2	0.5	1.5

Table 9: Calibrated expressions of $k_{y,prop}$ and $k_{z,prop}$

Interaction factor	Duplex	Ferritic
$k_{y,prop}$	For $\overline{\lambda}_y$ <1.3, $k_{y,prop} = 1 + 2.0\left(\overline{\lambda}_y - 0.3\right) n_y$	For $\overline{\lambda}_y$ <1.3, $k_{y,prop} = 1 + 1.6\left(\overline{\lambda}_y - 0.35\right) n_y$
	For $\overline{\lambda}_y$ ≥1.3, $k_{y,prop} = 1 + 2.0 n_y$	For $\overline{\lambda}_y$ ≥1.3, $k_{y,prop} = 1 + 1.52 n_y$
$k_{z,prop}$	For $\overline{\lambda}_z$ <1.2, $k_{z,prop} = 1 + 2.7\left(\overline{\lambda}_z - 0.5\right) n_z$	For $\overline{\lambda}_z$ <1.5, $k_{z,prop} = 1 + 2.2\left(\overline{\lambda}_z - 0.5\right) n_z$
	For $\overline{\lambda}_z$ ≥1.2, $k_{z,prop} = 1 + 1.89 n_z$	For $\overline{\lambda}_z$ ≥1.5, $k_{z,prop} = 1 + 2.2 n_z$

Table 10: Assessment of accuracy of proposed design rules for duplex stainless steel welded I-section beam-columns

Design method	Loading	Section class	N	ϵ_{av}	ϵ_{COV}	ϵ_{max}	ϵ_{min}
Proposal	Major axis bending and compression	Class 1 & 2	280	1.08	0.046	1.19	0.96
		Class 3	145	1.15	0.065	1.27	0.98
	Minor axis bending and compression	Class 1 & 2	280	1.09	0.061	1.39	0.96
		Class 3	145	1.25	0.055	1.37	0.99

Table 11: Assessment of accuracy of proposed design rules for ferritic stainless steel welded I-section beam-columns

Design method	Loading	Section class	N	ϵ_{av}	ϵ_{COV}	ϵ_{max}	ϵ_{min}
Proposal	Major axis bending and compression	Class 1 & 2	280	1.06	0.038	1.17	0.96
		Class 3	140	1.08	0.066	1.21	0.91
	Minor axis bending and compression	Class 1 & 2	280	1.09	0.075	1.50	0.94
		Class 3	140	1.25	0.065	1.42	1.08

Table 12: Reliability analysis of proposed design method for duplex and ferritic stainless steel welded I-section beam-columns

Loading	Stainless steel	Data	N	b	$k_{d,n}$	V_δ	γ^*_{M1}
Major axis bending and compression	Duplex	FE	420	1.10	3.44	0.060	1.09
		Experiments	5	1.18	3.44	0.021	0.97
		Experiments & FE	425	1.11	3.44	0.060	1.09
	Ferritic	FE	420	1.06	3.44	0.050	1.05
		Experiments	–	–	–	–	–
		Experiments & FE	–	–	–	–	–
Minor axis bending and compression	Duplex	FE	420	1.14	3.44	0.089	1.13
		Experiments	5	1.32	3.44	0.030	1.01
		Experiments & FE	425	1.15	3.44	0.090	1.13
	Ferritic	FE	420	1.14	3.44	0.096	1.10
		Experiments	–	–	–	–	–
		Experiments & FE	–	–	–	–	–